Ref. Ares(2018)5595206 - 31/10/2018

Grant Agreement No. 727348

Project Acronym:

SOCRATCES

Project title:

SOlar Calcium-looping integRAtion for Thermo-Chemical Energy Storage.

DELIVERABLE D3.2

Calciner Kinetics Model

Funding scheme:	Research and Innovation Action (RIA)		
Project Coordinator:	USE		
Start date of the project:	01.01.2018	**Duration of the project:**	36 months
Contractual delivery date:	Month 10		
Actual delivery date:	31.10.2018		
Contributing WP:	WP3		
Dissemination level:	*Public*		
Authors:	Tom Hills (Calix); Angeliki Lemonidou (AUTH); Luis Maqueda (CSIC); George Karagiannakis (CERTH)		
Contributors:	Jonatan Duran (CSIC), Athanasios Scaltsoyiannes & Andy Antzara (AUTH), Chrysa Pagkoura (CERTH)		
Version:	V 1.0		
Document name	**SOCRATCES Deliverable 3.2**		

Summary

Experiments determining the kinetic and cyclical behaviour of potential SOCRATCES calcium-based sorbents have been performed at three institutions: Aristotle University Thessaloniki (AUTH), the Centre for Research and Technology Hellas (CERTH), and Consejo Superior de Investigaciones Científicas (CSIC).

Part One explains experiments performed at AUTH. The sorbent was cycled between calcination and carbonation conditions in a fixed bed comprising mostly inert sand. The rate of calcination was measured, allowing for determination of the kinetic constants of two mechanistic models: the Prout-Tompkins Model (PTM) and the Generalised Random Pore Model (GRPM). These models follow different mechanistic routes but deliver similar results. The activation energies were determined to be 230 kJ/mol (PTM) and 168 kJ/mol (GRPM). In general, the GRPM better explained the kinetic behaviour at low extents of calcination but both models over-estimated the extent of calcination at higher extents. Furthermore, it can be used for predictive modelling of a greater range of conditions than the PTM. However, it is more complex and requires more sorbent characterisation to be performed before the kinetic constants can be extracted.

Part Two covers the study at CSIC. Similar work was performed, but in a thermogravimetric analyser. In these studies, the partial pressures of CO_2 were significantly higher, at 0.7 and 1.0 atm rather than 0.31 atm. It also differs from the AUTH work in that the temperature, rather than the atmosphere, was altered to move the sorbent between calcination and carbonation conditions. Good fits of the PTM with the experimental data were achieved, especially at slow rates of calcination. However, the rate of calcination was found to be significantly slower than that predicted by the GRPM using the constants derived from the AUTH work, in some cases by several orders of magnitude. The reason for this disparity will be investigated in the following months.

Part Three explains the work performed by CERTH in which the effect of fast calcination on the rate of CO_2 uptake and the total capacity of the sorbent was investigated. Although a fast calcination pre-treatment step increased the multi-cycle capacity and rate of uptake of dolomite, such an effect was not seen in limestone. The exact reason for this is not confirmed, but it is likely to relate to the micro/nano-structure of the non-carbonating magnesium component of the sorbent. The rate of heating during pre-treatment was not shown to have a large effect on the dolomite's performance, but pre-treatment in helium was found to improve performance. Further studies will be performed to investigate the effect of the rate of cooling and the dwell time during experiments. Sorbent characterisation analysis will be performed to better understand the nature of the cycled materials and provide information on the material activation mechanism observed for dolomite.

The results from all three parts of this deliverable will be used in the final calciner designs and the operation of the pilot plant.

TABLE OF CONTENTS

TABLE OF FIGURES

1. AIM OF THE DELIVERABLE

The aims of this deliverable are to:

i. Present the kinetic models and constants of laboratory experiments of the calcination of sorbent suitable for use in SOCRATCES;
ii. Determine optimum conditions for the calcination of sorbent;
iii. Explain how flash calcination affects the carrying capacity and rate of calcination of sorbents.

2. CALCINER CONCEPT

Calcination can occur in two vessels in SOCRATCES: the solar calciner, which is predominantly heated by concentrated solar power; and the electric calciner, which is predominantly heated by electrical resistance. The kinetics are not affected by the method of heat provision beyond any differences in temperature or flux profile that are inherent in the character of the energy vector. Both are Calix Flash Calciners (CFCs), where small limestone particles are heated using mostly radiation from calciner walls so that they heat up and calcine within a few seconds. This allows control of the atmosphere within the reactor.

The solar calciner can be operated in two modes: indirect, where the concentrated solar energy is absorbed in a cavity by the cavity wall. This cavity wall is surrounded by the calciner annulus through which the limestone passes vertically downwards. The outer wall of the annulus is not heated by solar power but may have some electrical heating to maintain the temperatures within the pilot-scale calciner. In the direct mode, the solar energy passes through a transparent window and directly impinges on the limestone as it falls, allowing a greater flux and higher effective temperature, but over a smaller area.

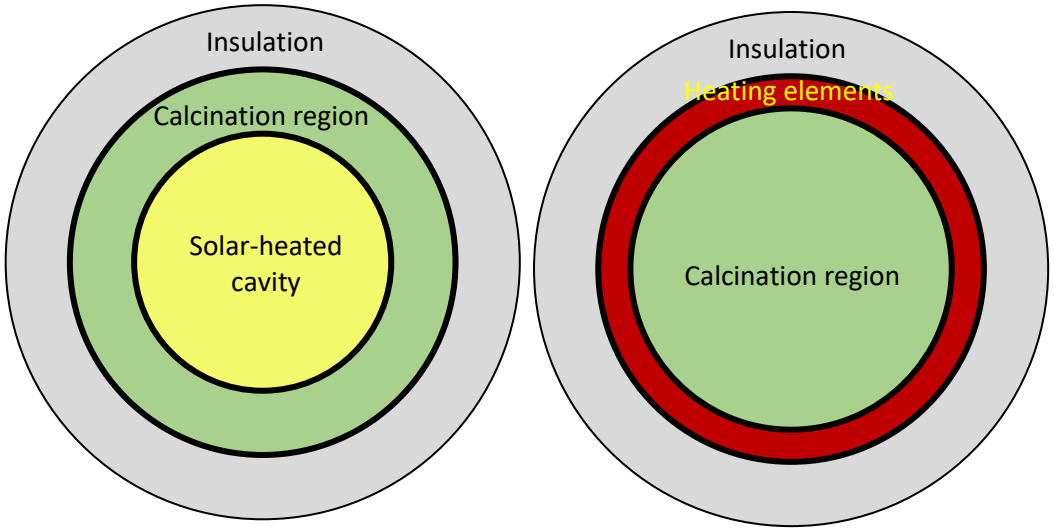

Figure 1 – Illustration of the Solar and Electric CFC cross-sections

This process is innovative because contemporary industrial-scale CSP systems only reach 700 °C due to the loss of efficiency that increases with increasing temperature. It is expected that the solar calciner will have to achieve wall temperatures of at least 950 °C to get sufficient heat transfer. The use of a cavity should help to reduce this loss.

The solar and electric CFCs will have the ability to inject other gases such as steam to lower the partial pressure of CO_2 and increase the rate of calcination at any specific temperature.

3. CALCINATION THEORY

This section covers calcination and two models which aim to explain it quantitatively. They approach the problem from two different angles. These are the Generalised Random Pore Model (GRPM), which uses surface area on the outside of the particle and within the pores, as well as a reaction front velocity, to calculate the rate of calcination. The Prout-Tompkins Model (PTM) approaches it using an autocatalysis technique, where calcination starts at nucleation points and spreads through the particle from there.

3.1. The Generalised Random Pore Model (GRPM)

There are two common geometry models used in the literature to describe calcination. The Shrinking Core Model (SCM) assumes that the particle is impervious, and the reaction proceeds from outer surface of the particles inwards. The Random Pore Model (RPM) assumes that the particle is porous and the reaction proceed uniformly through the particle by reaction fronts that proceed from the surface of every pore, in which there is an increase in the pore radius of the limestone as the reaction proceeds. The basic theory developed in this work is a generalisation of the RPM of Bhatia et al. [1], and Gavalas [2]. The calcination changes during the reaction because the overlap of the expanding pores evolves in a non-linear fashion, through the statistics of pore intersections [3]. The GRPM unifies the RPM with the SCM. It was devised and developed by Mark Sceats of Calix [4].

The premise of the RPM is that the reaction coordinates are all of the pore radii. The simplification of the model for calcination is that all the pores change radius uniformly at the same rate. With the assumption of uniform temperature and pressure, the pore radius change is also uniform within in the particle. However, a significant reaction coordinate is the depth from the initial particle surface. It is generally neglected in the RPM. The particle surface is the nominal surface of "interparticle pores". A collection of "particles" is therefore a particle in which these interparticle pores are simply another set of pores of the collection. Logically, limestone at the particle surface is no different from limestone at an internal surface (neglecting grinding effects).

The RPM asserts that all the particle pores expand at the same rate, and, self-consistently, this include the pores that are the spaces between the "particles". The reaction front for calcination for this pore moves into the particle as the reaction proceeds, and the reaction coordinate is the depth from the particle surface. The GRPM combines both these manifestations of calcination.

The GRPM requires knowledge of the particle size distribution, pore volume and total particle and pore surface area. From this, the contributions of the geometrical surface area (i.e. the outer surface of the particle) S_{g0} and the pore surface area S_{A0} can be determined. The mean pore diameter, which all pores are assumed to have, can also be calculated, as can the pore length $L_A(\zeta)$. The particle depth distribution $PDD_A(\zeta)$ is a function of the particles size distribution.

In summary, the final $GRPM$ expression for extent of calcination α of homogeneous particles used here is

$$\alpha(q_A) = \int_0^{q_A} PDD_A(\zeta)d\zeta + \{1 - exp[-S_A(\zeta)q_A - \pi L_A(\zeta)q_A^2]\} \int_{q_A}^{\zeta_{max}} PDD_A(\zeta)\, d\zeta.$$

The first term on the right hand side calculates the SCM part of the model and the second term calculates the RPM part of the model, minus the parts which would have otherwise have been calcined by the SCM. The terms q_A and ζ are the extents to which the reaction front has reached from the pore surfaces and the particle surface, respectively. In this work, these values are assumed to be equal. They are dependent on the velocity of the reaction front, k, and the duration of calcination, t.

As a velocity, k has the units ms^{-1}. It is dependent upon the same parameters as most rate constants for calcination, including temperature T, partial pressure of CO_2 p_{CO2} and partial pressure of steam p_{H2O}. The velocity of calcination can be calculated as a value for a particular system which is then modified by factors for temperature and partial pressures of carbon dioxide and steam. In other words,

$$k_A\left(T, p_{CO_2}, p_{H_2O}\right) = A \times f(T) \times f(p_{CO_2}) \times f(p_{H_2O})$$

Data show that the temperature dependence is an Arrhenius function [5], i.e.

$$f(T) = B \times e^{\frac{E_A}{RT}}$$

The values of A*B = k_0 and E_A are extracted from the model by performing experiments at different temperatures. This is performed in Section 6.1.

Since the calcination reaction is reversible, the rate of calcination is actually a net rate of calcination and carbonation. As such, it is dependent on the partial pressure of CO_2 and the equilibrium and saturation pressures of CO_2. The saturation pressure has been determined to be approximately equal to the equilibrium pressure under the typical circumstances of calcination. Making another approximation for a parameter based on the size factor of the CaO* intermediate species $N_v = 1$ [6], the model becomes

$$f(p_{CO_2}) = \left(1 - \theta_{CO_2}(T, p_{CO_2})\right)\left[1 - \frac{p_{CO_2}}{p_{CO_2,eq}(T)}\right]$$

$$\theta_{CO_2}(T, p_{CO_2}) = \frac{\frac{p_{CO_2}}{P_{CO_2,eq}(T)}}{1+\frac{p_{CO_2}}{P_{CO_2,eq}(T)}}$$

Steam has been shown to have a catalytic effect on the rate of calcination [7], [8]. This is a function of the saturation pressure of steam and the partial pressure of steam.

$$f(p_{H_2O}) = \left[1 + \theta_{H_2O}(T, p_{CO_2}, p_{H_2O})\Delta(T)\right]$$

With:

$$\theta_{H_2o}(T, p_{H_2O}) = \frac{1}{1+\frac{p_{H_2O}}{P_{H_2O,sat}(T)}}$$

$$\Delta(T) = 14150\ exp\left\{-\frac{6014}{T}\right\} \qquad [7]$$

$$p_{H_2O,sat}(T) = 3.33\ 10^8 \exp\left\{-\frac{12594}{T}\right\} \text{ kPa.} \qquad [8]$$

Putting all the parts together gives the final model:

$$k_A(T, p_{CO_2}, p_{H_2O}) = k_0\ e^{-\frac{24658}{T}}\left[1 - \theta_{CO_2}(T, p_{CO_2})\right]^{N_v}\left[1 + \theta_{H_2O}(T, p_{CO_2}, p_{H_2O})\Delta(T)\right]\left[1 - \frac{p_{CO_2}}{p_{CO_2,eq}(T)}\right]$$

The development of the model is explained in more detail in the Annex (Section 0).

3.2. Prout-Tompkins Model

In homogeneous kinetics, autocatalysis occurs when the products catalyse the reaction; this occurs when the reactants are regenerated during a reaction in what is called “branching”. The reactants will eventually be consumed and the reaction will enter a “termination” stage where it will cease. A similar observation can be seen in solid state kinetics. Autocatalysis occurs in solid-state kinetics if nuclei growth promotes continued reaction due to the formation of imperfections such as dislocations or cracks at the reaction interface (i.e., branching). Termination occurs when the reaction begins to spread into material that has decomposed. Prout and Tompkins derived an autocatalysis model for the thermal decomposition of potassium permanganate which produced considerable crystal cracking during decomposition [9], [10]. In autocatalytic reactions, the nucleation rate can be defined by

$$\frac{dN}{dt} = k_N N_0 + (k_B - k_T)N \qquad (1)$$

where, k_B is the branching rate constant and k_T is the termination rate constant. If $k_N N_0$ is neglected, eq. 1 becomes

$$\frac{dN}{dt} = (k_B - k_T)N \qquad (2)$$

This could occur in one of two cases: (1) k_N is very large so that initial nucleation sites are depleted rapidly and calculations of dN/dt are valid for time intervals after N_0 sites are depleted. (2) k_N is very small so that $k_N N_0$ can be ignored. The reaction rate is related to number of nuclei by

$$\frac{da}{dt} = k'N \quad (3)$$

where, k' is the reaction rate constant. Prout and Tompkins found that the shape of R vs time plots for the degradation of potassium permanganate was sigmoidal [9]. Therefore, an inflection point exists (α_i,t_i) at which dN/dt will change signs. From the boundary conditions that need to be satisfied at that inflection point (i.e., $k_B = k_T$), the following can be defined:

$$k_T = k_B \frac{a}{a_i} \quad (4)$$

Substituting eq. 4 into eq. 2 gives

$$\frac{dN}{dt} = k_B \left(1 - \frac{a}{a_i}\right) N \quad (5)$$

Since dN/dα=(dN/dt)*(dt/dα), eq. 6 can be obtained:

$$\frac{dN}{dt} = k'' \left(1 - \frac{a}{a_i}\right) N \quad (6)$$

where k''=k_B/k'. Assuming k_B is independent of α, separating variables in eq 6 and integrating gives:

$$N = k'' \left(a - \frac{a^2}{2a_i}\right) N \quad (7)$$

Substituting eq. 7 into 3 gives

$$\frac{da}{dt} = k_B \left(a - \frac{a^2}{2a_i}\right) N \quad (8)$$

Since Prout and Tompkins assumed that α_i= 0.5, eq. 8 reduces to:

$$\frac{da}{dt} = k_B a(1 - a) \quad (9)$$

Eq. 9 has been used by Valverde et al. [11] for describing calcination reaction kinetics. After integration eq. 9 gives:

$$a = \frac{1}{1+\exp(-r(t-t_0))} \quad (10)$$

Where r (1/s) is the intrinsic reaction rate, while t_0 is the time when α=0.5.

PART ONE: KINETIC EXPERIMENTS IN A FIXED BED (AUTH)

4. FIXED-BED EXPERIMENTAL SETUP

4.1. Experimental apparatus

The experimental apparatus used for the kinetic experiments at AUTH is shown in Figure 9. The continuous flow unit which operates at 1.55 bara consists of the gas feed inlet section, the reactor and the product analysis section. The incoming gases are controlled by mass flow controllers and are pre-mixed before entering the reactor. A fixed bed quartz reactor (10 mm internal diameter), equipped with a coaxial thermocouple for temperature monitoring, was used for the testing. The reactor is heated electrically by a tubular furnace, with three independently controlled temperature zones. The hot gases exiting the reactor are cooled down to room temperature and continuously analyzed by a mass spectrometer (MS) (Omnistar ™ GSD 320, PFEIFFER).

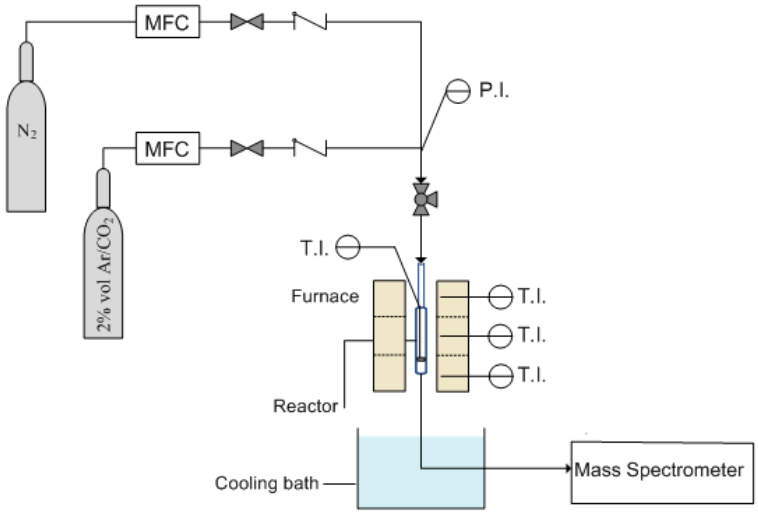

Figure 2 – Schematic diagram of the apparatus used for the kinetic experiments.

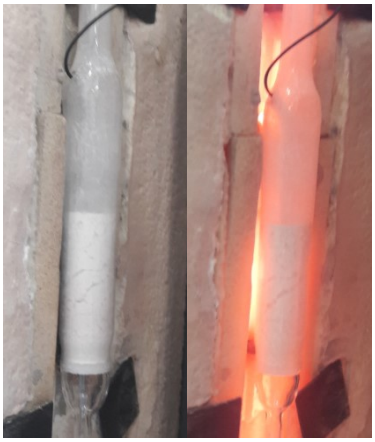

Figure 3 – Fluidisation test of limestone (Granicarb 0.1/0.8 sample, particle size <45μm) at 300 °C (left) and 800 °C (right).

The AUTH team examined the fluidisation ability of limestone particles with size less than 106 μm. Flow channelling and no fluidization were observed for particles with size less than 45 μm at both low (300 °C) and higher (800 °C) temperatures as it is shown in Figure 7. After the test, it was also observed that the used material was loosely agglomerated. Larger particle size range (75–106 μm) showed good fluidisation behaviour

at temperatures less than 600 °C. At higher temperatures it was also agglomerated and the fluidization stopped.

In contrast, dolomite samples with particle size between 150 and 200 μm presented adequate fluidisation performance at low and high temperature range with minimum attrition. Fluidisation velocities starting from 3 to 15 times the minimum fluidisation velocity (U_{mf}) have been applied. The conversion of the dolomite as a function of cycling and variation in U_{mf} and carbonation/calcination temperature is presented in Figure 8.

Zero carbonation rate was observed at temperatures over 900 °C due to thermodynamic limitations.

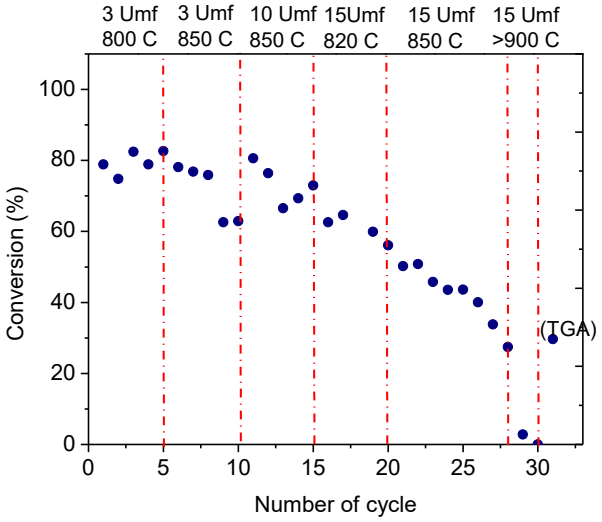

Figure 4 – Conversion though carbonation/calcination cycles of dolomite with particle size of 150–200 μm at various temperatures and fluidization rates

With regard to calcination kinetics, the experimental work was carried out in a fixed bed reactor unit instead of a fluidised bed, as it is a much simpler system and can provide more accurate results.

4.2. Experimental protocol

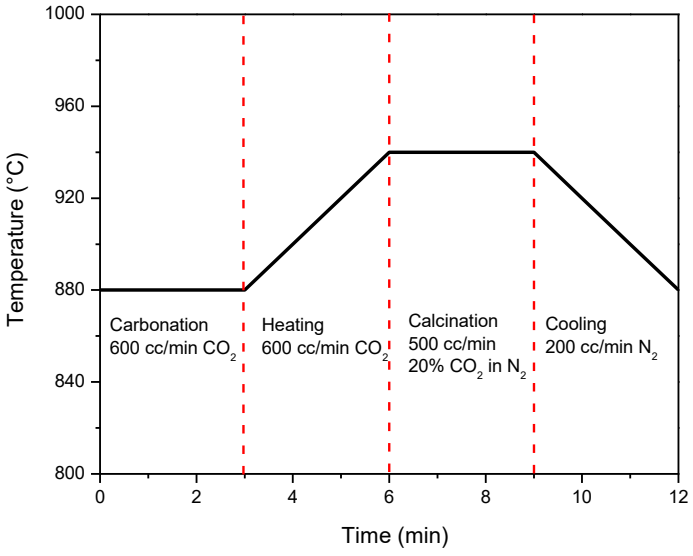

Figure 5 – Schematic diagram of the experimental stages for the calcination kinetics measurements at 940 °C under 500 cc/min 20%vol CO_2 in N2.

The sorbent materials were sieved in the range of $45 < d_p < 75$μm and about 100 mg mixed with 1.5 g of quartz with particle size of $100 < d_p < 180$ μm were loaded in the reactor. The reactor was heated (heating rate of 20 °C/min) up to the carbonation temperature (e.g. 880 °C) under N_2 flow of 200 cc/min, so that full calcination

is taking place (pre-treatment). When the carbonation temperature was reached, carbonation initiated by switching the flow from pure N_2 to 600 cc/min of CO_2 (containing 2%vol. Ar used as an internal standard).

The carbonation stage was carried out for 3 mins isothermally. Subsequently the reactor was heated to the calcination temperature (e.g. 940 °C) under CO_2 flow – in order to avoid calcination – with a heating rate of 20°C/min. When calcination temperature was reached, the calcination phase took place for 3 mins by switching the flow to 20%vol. CO_2/N_2 (500 cc/min). The CO_2 flow during calcination also contained 2%vol. Ar. Given that the Ar flow was constant, the flow ratio of CO_2/Ar increased when calcination reaction was taking place. The flow changes were detected by the mass spectrometer. Temperature in the reactor was also recorded during the whole procedure. Subsequently, a flow of 200 cc/min of pure N_2 was introduced into the reactor to verify full calcination while simultaneously the reactor was cooled at the carbonation temperature under the same flow and the cycle was repeated. This procedure (one cycle) is presented in Figure 5.

5. FIXED-BED CALCINATION RESULTS

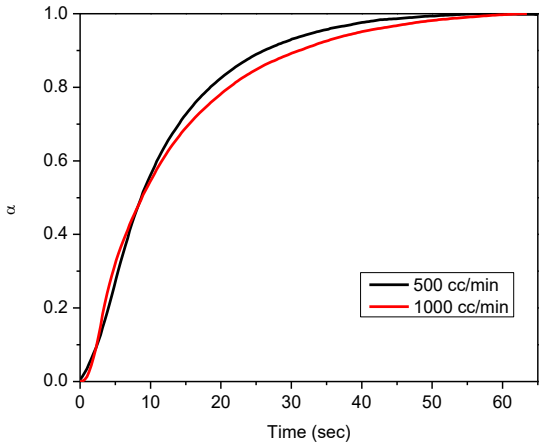

Figure 6 – Calcination of limestone under two different gas flow rates. Material: Granicarb 0.1/0.8 (OMYA) (45–75 μm); Calcination conditions: temperature: 900 °C; gas flow rates: 500 or 1000 cc/min (20 % CO_2 in N_2); sample mass: 100 and 200 mg respectively.

Figure 11 shows the calcination conversion-time diagram for two different flow conditions. The results are presented not as conversion (X) but as fractional conversion (α) based on the carbonated quantity, as shown in the model theory section. Increasing the gas flow over 500 cc/min has no effect on the reaction rate. Above that limit the mass and heat transfer phenomena are overcome and the kinetic study is valid.

5.1. Effect of Temperature

Experiments were conducted varying the calcination temperature in order to evaluate its effect on the calcination rate. The total gas flow was 500 cc/min (20% CO_2 / N_2) in every case. Increasing the temperature, the calcination rate also increases (Figure 12). Calcination is an endothermic reaction and is favoured by increasing the reaction temperature. Two different materials were used, a limestone (Omya Granicarb 0.1/0.8 (45–75 μm)) and a dolomite (Omya Microdol 1KN (45–75 μm)) under the same reaction conditions.

5.2. Effect of Material

Two different materials were used, a limestone (Omya Granicarb 0.1/0.8 (45–75 μm)) and a dolomite (Omya Microdol 1KN (45–75 μm)) under the same reaction conditions. In both calcination temperatures (900 and 925 °C) dolomite exhibited higher reaction rates than limestone, probably due to the larger surface area (Figure 13). In addition, MgO content renders dolomite a much more sintering resistant material compared to limestone, achieving high conversions (>80% during the first 5 cycles) (Figure 14). This could give compensation for the lower CaO concentration (~67% wt. after calcination).

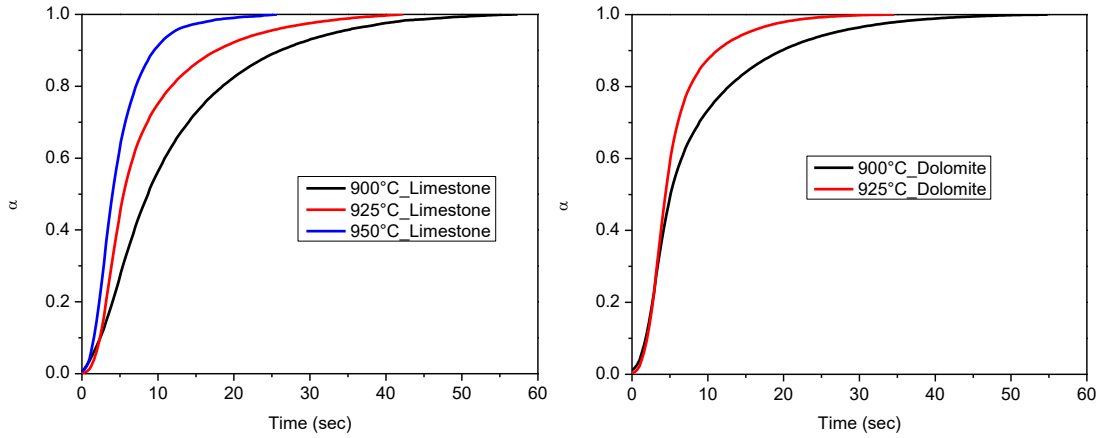

Figure 7 – Calcination of limestone at 900, 925 and 950 °C (left) and dolomite at 900 and 925 °C (right). Calcination conditions: materials: Granicarb 0.1/0.8 (OMYA) (45–75 µm) (left), Microdol1KN (OMYA) (45–75 µm) (right); gas flow rate: 500 cc/min (20 % CO_2 in N_2); sample mass: 100 mg.

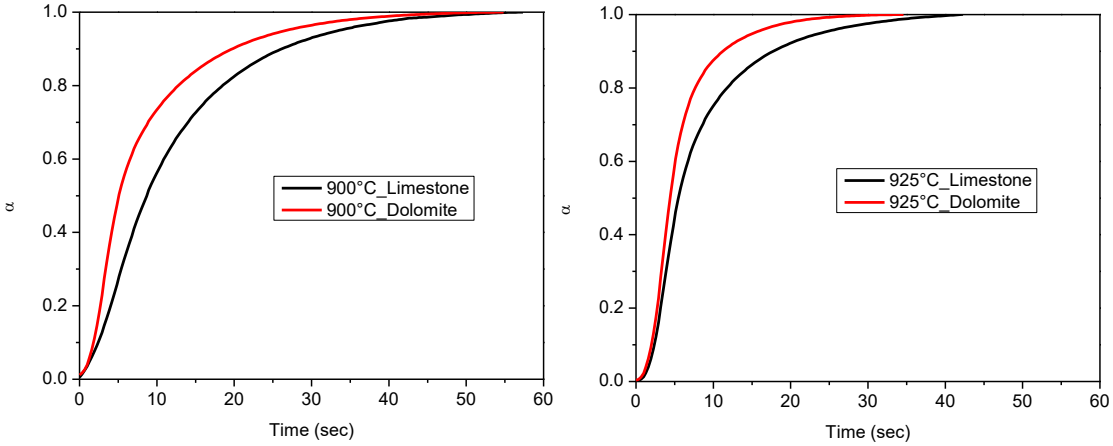

Figure 8 – Calcination of limestone and dolomite at 900 °C (left) and 925 °C (right). Calcination conditions: materials: Granicarb 0.1/0.8 (OMYA) (45–75 µm), Microdol1KN (OMYA) (45–75 µm); gas flow rates: 500 cc/min (20 % CO_2 in N_2); sample mass: 100 mg.

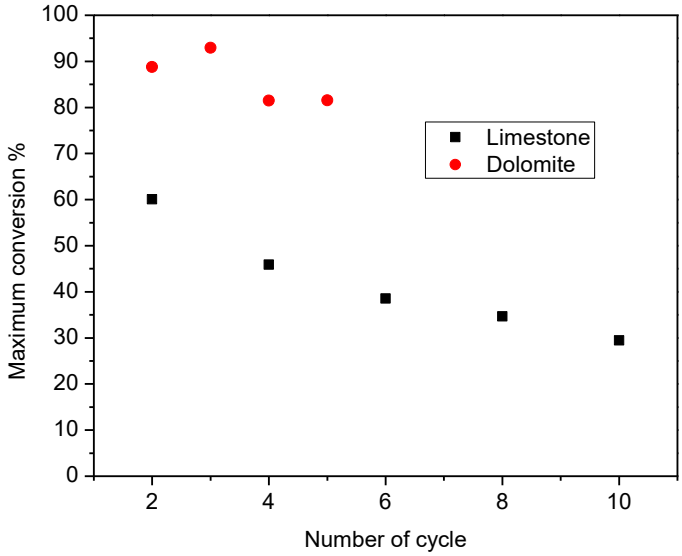

Figure 9 – Evolution of maximum conversion of limestone and dolomite through the cycles. Materials: Granicarb 0.1/0.8 (OMYA) (45–75 µm), Microdol1KN (OMYA) (45–75 µm); sample mass: 100 mg; Calcination conditions: Temperature: 880 °C; gas flow rate: 500 cc/min (20% CO_2 in N_2); Carbonation conditions: Temperature: 880 °C; gas flow rate: 600 cc/min CO_2.

5.3. Effect of Sweep Gas Composition

Two different gases were used for the dilution of CO_2 in the feed of the reactor, namely N_2 and He, in order to examine the influence of the carrier gas on the calcination rate. In both cases the CO_2 concentration was the same (20%vol.). As can be seen in Figure 15, no difference was observed in the reaction rate by substituting nitrogen with helium. Some researchers refer that He enhances the calcination rate due to its higher thermal conductivity compared to N_2, but this is not the case when heat transfer is not controlling the rate. Borgwardt [12] also concluded in the same result after using three different sweep gases during calcination (N_2, He and Ar).

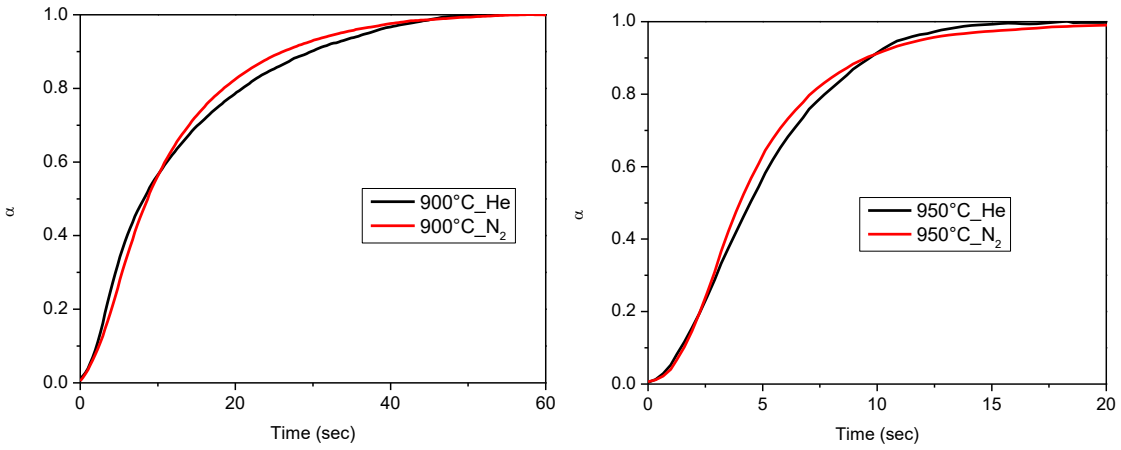

Figure 10 – Calcination of limestone under N_2 and He at 900 °C (left) and 950 °C (right). Calcination conditions: material: Granicarb 0.1/0.8 (OMYA) (45–75 μm); gas flow rate: 500 cc/min (20 % CO_2 in N_2 or He); sample mass: 100 mg.

6. ANALYSIS OF PART ONE RESULTS – FITTING TO MODELS

Two different kinetic models were used for describing the evolution of the calcination conversion as a function of time in the fixed bed experiments, namely the Prout-Tompkins (P-T) and the Generalized Random Pore Model (GRPM). The fitting procedure derived the intrinsic reaction rate parameter k. For a given value of k, the two intrinsic rate parameters can be calculated, the pre-exponential factor (k_0) and the activation energy of the reaction (E_a) using the Arrhenius equation.

6.1. Generalized Random Pore Model (GRPM)

According to the GRPM, the calcination rate is proportional to the available surface area for reaction. It uses the initial material properties (Table 1) for the prediction of the reaction rate, so the input information is the BET surface area, the pore volume and the particle size distribution (PSD). The material that was used in the kinetics experiments had a very narrow particle size range (45–75 μm), so it is a good approximation to use a single mean value of 60 μm, instead of a PSD for the calculations. The equations used for the material initial properties calculations are:

$S_{g0} = \frac{6}{d_p}$, geometrical surface area

$S_{A0} = S_{BET} - S_{g0}$, pores surface area

$\sigma_0 = \frac{2V_p}{S_{A0}}$, mean pore radius

$L_0 = \frac{S_{A0}}{2\pi\sigma_0}$, mean pore length

$\varepsilon_0 = \frac{\rho_b V_p}{1+\rho_b V_p}$, porosity

Table 1 – Initial values of the limestone properties that were used in the GRPM.

Property	Value
Bulk density, ρ_b (g/m^3)	2.71E+06
BET surface area (m^2/g)	0.4168
BET surface area (m^2/m^3)	1108700
Geometrical surface area, S_{g0} (m^2/m^3)	100000
Mean pores surface area, S_{A0} (m^2/m^3)	1008700
Mean particle diameter, d_p (m)	0.00006
Mean Pore Length, L_{A0} (m/m^3)	4.39E+12
Pore Volume, (m^3/g)	6.93E-09
Mean Pore Volume, V_p (m^3/m^3)	1.84E-02
Mean pore radius, σ_0 (m)	3.66E-08
Porosity, ε_0	0.018

The bulk density ρ_b refers to the density of calcite and was found in the literature [13].

The expression of the conversion versus time according to the GRPM is:

$$\alpha(t) = \int_0^t k\frac{6[\mathrm{d}_p - 2kt]^2}{\mathrm{d}_p^3}dt + \{1 - exp[-S_{A0}kt - \pi L_{A0}(kt)^2]\}\int_t^{d_p/2k} k\frac{6[\mathrm{d}_p - 2kt]^2}{\mathrm{d}_p^3}dt$$

The first term of the sum arises from the propagation of the reaction front from the particle surface, while the second term arises from the homogenous calcination from the internal pores of the particle.

The reaction rate k (m/s) is the fitting parameter of the above equation to the experimental data (Table 2).

Table 2 – Values of intrinsic reaction rate k obtained from the fitting of the GRPM with the experimental data.

T (°C)	900 °C	925 °C	950 °C
k (nm/s)	18.5	28.5	43.5

The intrinsic reaction rate k is a function of the calcination temperature, CO_2 partial pressure and the steam partial pressure:

$$k(T, p_{CO_2}, p_{H_2O}) = k_A(T)\left[1 - \theta_{CO_2}(T, p_{CO_2})\right]^{N_v}\left[1 + \theta_{H_2O}(T, p_{CO_2}, p_{H_2O})\Delta(T)\right]\left[1 - \frac{p_{CO_2}}{p_{CO_2,eq(T)}}\right] \quad \text{(eq. 14)}$$

With

$$\theta_{CO_2}(T, p_{CO_2}, p_{H_2O}) = \frac{\frac{p_{CO_2}}{P_{CO_2,eq(T)}}}{1+\left[\frac{p_{CO_2}}{P_{CO_2,eq(T)}} + \frac{p_{H_2O}}{P_{H_2O,sat(T)}}\right]}$$

$$\theta_{H_2O}(T, p_{CO_2}, p_{H_2O}) = \frac{\frac{p_{H_2O}}{P_{H_2O,sat(T)}}}{1+\left[\frac{p_{CO_2}}{P_{CO_2,eq(T)}} + \frac{p_{H_2O}}{P_{H_2O,sat(T)}}\right]}$$

The four parameters are:

$$k_A(T) = k_0\, exp\left[-\frac{E_a}{RT}\right] \text{ m s}^{-1} \quad \text{(eq. 15)}$$

$$p_{CO_2,eq}(T) = 4.137\ 10^9 \exp\left\{-\frac{20474}{T}\right\} \text{ kPa [14]}$$

$$p_{H_2O,sat}(T) = 3.33\ 10^8 \exp\left\{-\frac{12594}{T}\right\} \text{ kPa}$$

$$\Delta(T) = 14150\ exp\left\{-\frac{6014}{T}\right\}$$

where the temperature is in Kelvin and the gas pressures are in kPa.

N_ν is a variable which aims to account for variability of the parameters on the properties of limestone. Based on the literature, the value of N_ν is of order 0.75–1.50 for limestone. In the calculations was taken the value $N_\nu = 1$.

The above equations include the pre-exponential factor (k_0) and the activation energy of the reaction (E_a) which are the derived parameters of the model. The results of the fitting of the GRPM with the experimental data are shown in Figure 11:

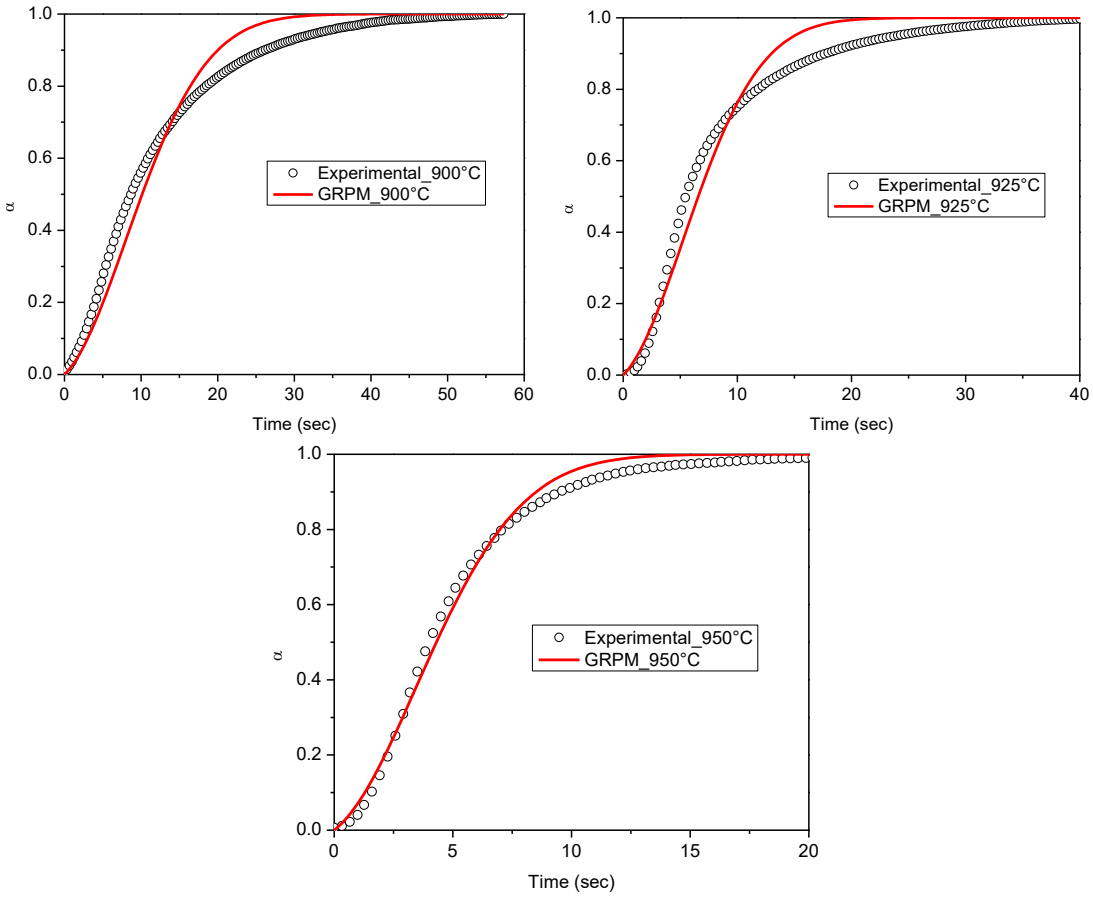

Figure 11 – Fitting of the GRPM with the experimental data for calcination of limestone at 900, 925 and 950 °C.

The GRPM describes adequately the experimental data for conversions up to 0.7–0.8. For higher conversions the model overestimates the conversion value compared to the actual. This deviation maybe occurs due to mass or heat transfer phenomena through the CaO product layer which decrease the reaction rate. Another theory is that there is sintering of the calcium carbonate before it calcines, thus reducing the surface area through which the reaction front can travel. The GRPM takes into account only the surface reaction and assumes homogeneous conditions (temperature, CO_2 partial pressure) in the pores, which may not be accurate at high conversions.

The activation energy and the pre-exponential factor of the calcination reaction are E_a=130 kJ/mol and k_0 = 0.021 ms^{-1} respectively. Thus,

$$k_A(T) = 0.021\ exp\left[-\frac{130}{RT}\right]\ \text{m s}^{-1}$$

Figure 17 shows the temperature dependence of k_A .

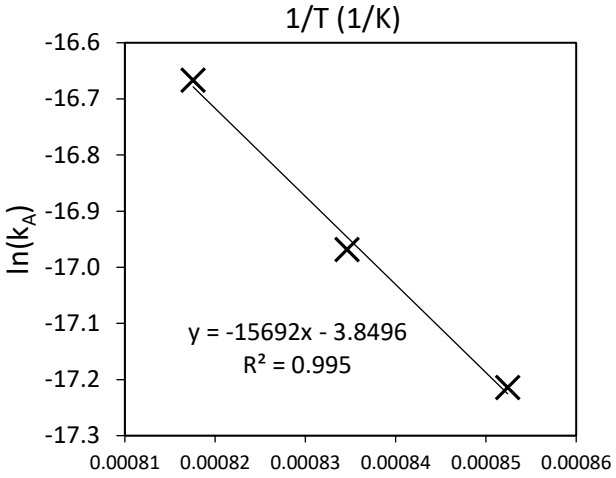

Figure 17 – Logarithm of reaction rate ln(k_A) as a function of 1/T derived from eq.15 of the GRPM.

6.2. Prout-Tompkins (P-T) model

The second model that was used for describing the calcination kinetics was adopted from Valverde et al. [11]. The mechanistic part is consistent with the Prout-Tompkins model:

$$a(t) = \frac{1}{1+ e^{-k(t-to)}}$$

The fitting parameter of the model is again the intrinsic reaction rate k (1/sec). Table 3 summarizes the values of k obtained from the fitting procedure.

Table 3: Values of intrinsic reaction rate k obtained from the fitting of the P-T model with the experimental data.

T (°C)	900 °C	925 °C	950 °C
k (1/s)	0.18	0.31	0.57

The mathematical generic expression that represents the reaction rate of gas-solid heterogeneous reactions is a function temperature and CO_2 partial pressure:

$$k \approx k_0 e^{-\frac{E_a}{RT}}\left(1-\frac{P}{P_{eq}}\right)\left(\frac{1}{1+(\frac{P}{P_{eq}})e^{\Delta S_1^O/R}e^{-\Delta H_1^O/RT}}\right) \qquad \text{(eq.19)}$$

Where

$$k_A(T) = k_0\ exp\left[-\frac{E_a}{RT}\right] \qquad \text{(eq.20)}$$

where E_a is the calcination activation energy, k_0 is a pre-exponential factor, and R the gas constant. The subscript 1 refers to the calcination reaction.

The CO_2 equilibrium partial pressure was calculated using the following equation:

$$P_{eq} = Ae^{-a/T}$$

The values for reaction enthalpies, entropies, and activation energies required for the calculation of the reaction rate were acquired from thermochemical data and are summarized in Table 4. The results of the fitting of the P-T model with the experimental data are shown in Figure 12.

Table 4: CO_2 Values of Enthalpy–Entropy changes in the chemical decomposition and desorption stages and activation energies.

Parameter	Value
ΔH^0_r (kJ/mol)	180
ΔH^0_1 (kJ/mol)	160
ΔH^0_d (kJ/mol)	20
E_d (kJ/mol)	20
E_2(kJ/mol)	20
ΔS^0_r (kJ/(mol K))	0,16
ΔS^0_1 (kJ/(molK))	0,068
ΔS^0_d (kJ/(molK))	0,092
R (kJ/(molK))	0,008314
A (atm)	40830000
a (K)	20474

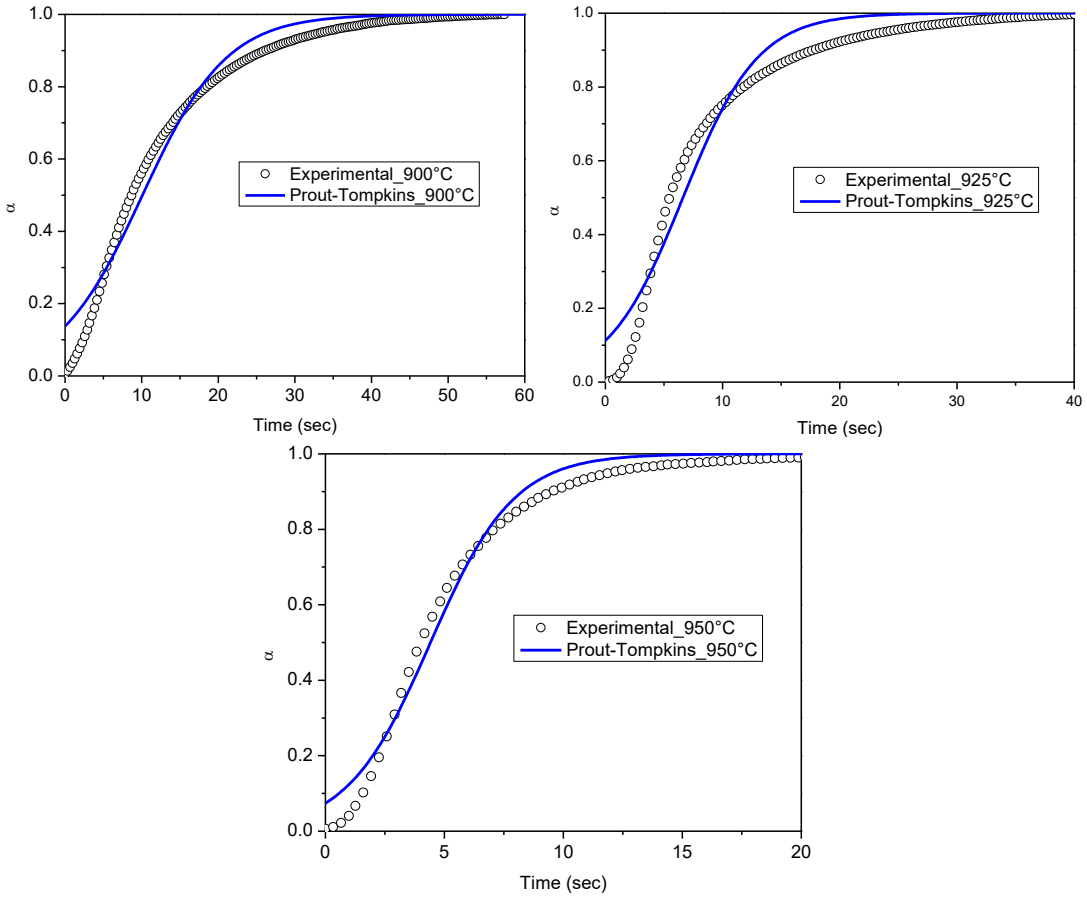

Figure 12 – Fitting of the P-T model with the experimental data for calcination at 900, 925 and 950°C.

The P-T model is a simple sigmoidal equation and deviates from the experimental data in two regions. The predicted conversion at t=0 is not zero and at high conversion has the same behaviour as the GRPM,

overestimating the conversion values. In general, the more "sigmoidal-like" the experimental data curve is, the better the fitting with the P-T model.

The activation energy and the pre-exponential factor of the calcination reaction (eq. 15) derived from the Prout-Tompkins model are E_a=230 kJ/mol and $k_0 = 4.69 * 10^9 s^{-1}$ respectively. Thus, eq. 20 transforms to:

$$k_A(T) = 4.69 * 10^9 \, exp\left[-\frac{230}{RT}\right] \ s^{-1}$$

Figure 13 shows the temperature dependence of the reaction rate k_A .

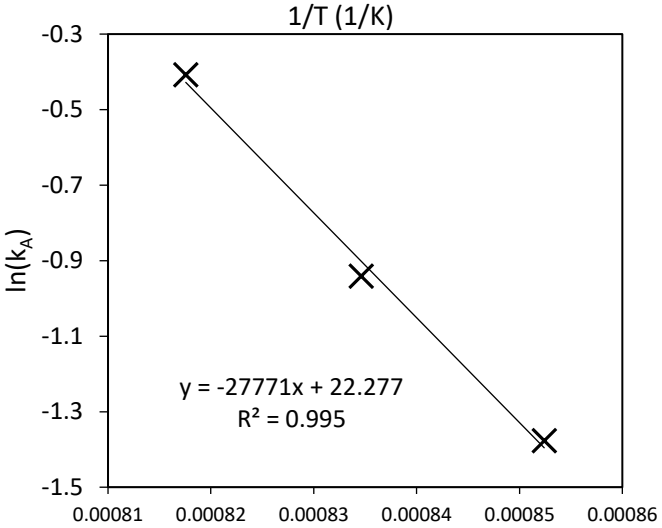

Figure 13 – Logarithm of reaction rate ln(k_A) as a function of 1/T derived from eq. 20 of the P-T model.

6.3 Comparison of the two models

Regarding the conceptual basis of the two models, GRPM is based on the prediction of the available reaction surface area from the initial value (S_{BET}). This comprises some risks on how accurate these measurements are because of the very low surface area of the limestone (usually < 1 m^2/g, in this case 0.41 m^2/g). Apart from that, it contains a solid theory on the evolution of the surface area during the reaction, increasing, of course, the complexity of the model. The Prout-Tompkins is a much simpler model (basically a sigmoidal curve) easy to use, but with more disadvantages on how adequately approaches the reality. Accordingly, the rate is proportional to the quantity that has reacted (α) and also proportional to the one left (1-α), but the experimental results deviate from that sigmoidal fashion.

Generally, the two models provide a good fitting to the experimental data obtained from a fixed bed reactor apparatus (Figure 18). In such a reactor type, the flow is passing through the sample resulting in efficient gas-solid contact and very fast reaction rates, in the order of magnitude of a few seconds. The activation energy of the reaction is equal to 130 and 230 kJ/mol according to the GRPM and the P-T model respectively. These values are not readily comparable because they are derived from different expressions of k (eq. 14 and eq. 19). If the same expression used (e.g. eq. 19) then k_A for GRPM becomes:

$$k_A(T) = 0.41 \, exp\left[-\frac{162}{RT}\right] \text{ m/s}$$

Where E_a=162 kJ /mol and k_0=0.41 m/s.

Using the same $k_A(T)$ expression (eq. 19) the activation energy values are comparable (GRPM: E_a=162 kJ /mol, P-T: E_a=230 kJ). This large difference is probably due to the deviations between the two models, especially in the case of 900 °C. Despite that difference, the two values are close to other found in the literature (Valverde et al. [11]: 180 kJ/mol, Borgwardt [12]: 205 kJ/mol). As it was mentioned previously, the GRPM describes

better the experimental data for conversions up to 0.7–0.8. Both models overestimate the conversion at high conversions probably due to mass or heat transfer phenomena arising from the produced CaO layer.

Both models express the apparent reaction rate (da/dt) to be proportional to the intrinsic reaction rate k, which is the fitting parameter. More specifically: (da/dt)=f*k. The rate k is in m/s for the GRPM and in 1/s for the P-T model. The function (f) is also completely different in the two models, so the derived values of k from the two models are not comparable.

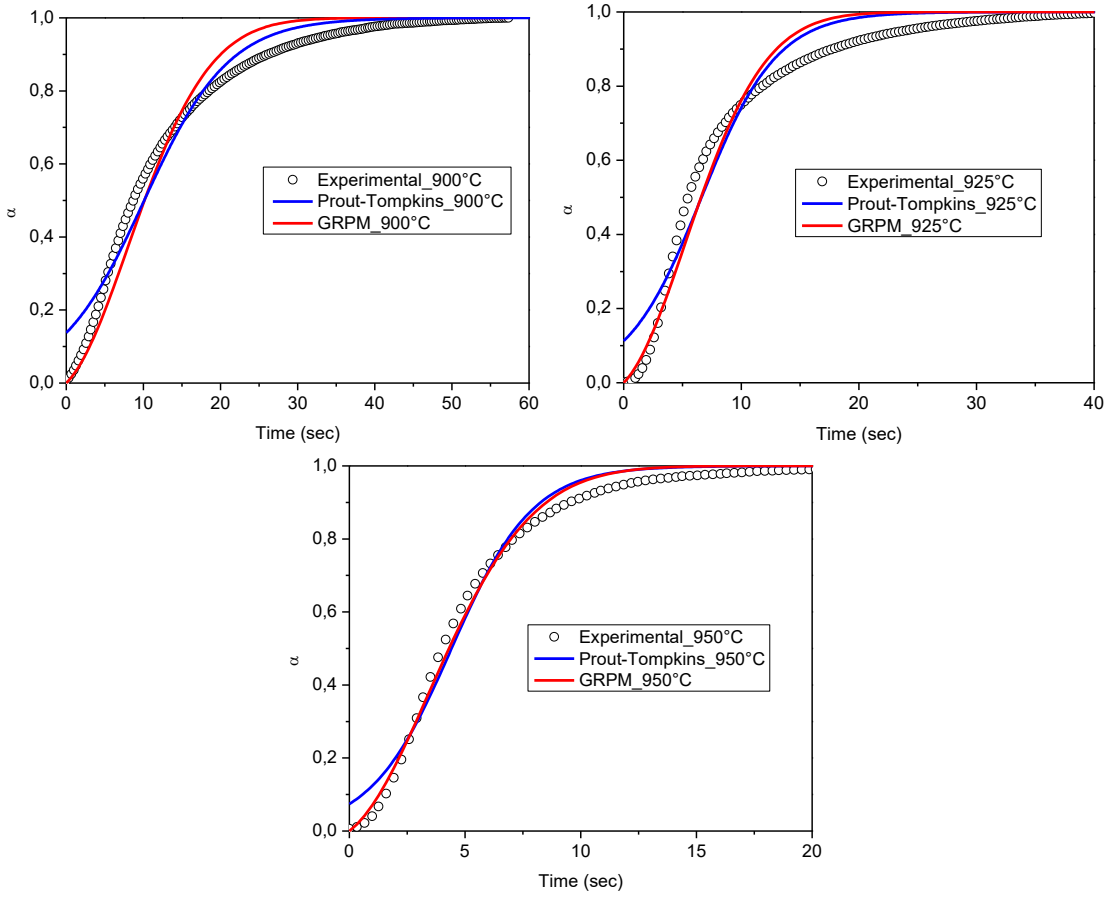

Figure 14: Comparison of the GRPM and the P-T model for calcination of limestone at 900, 925 and 950 °C.

7. APPLICATION OF THE MODELS TO SOCRATCES CONDITIONS

The experiments shown above were performed in 20% CO_2, but the atmosphere in the SOCRATCES calciners are likely to be 100% CO_2, at least for some experiments. The GRPM can be applied to these conditions now that the necessary parameters have been calculated.

It can be seen that the rate of calcination is greatly reduced when more CO_2 is present, especially in the 900 °C case. This is to be expected. For the GRPM, the extent of calcination at 925 °C can be taken to be acceptable, although higher levels would be desirable to improve the efficiency of the plant. Nevertheless, it can be said that the GRPM predicts that, for particles of 45–75 µm, temperatures of more than 925 °C will be required for at least 30 seconds. It will be necessary to get the particles to that temperature, which will take time and energy as well.

The Prout-Tompkins model, although less complex, cannot predict rates of calcination in 100% CO_2 with data from only 20% CO_2 atmospheres because of the dependence on t_0, which is empirically determined.

Table 5: Extent of calcination of limestone in 1 atm CO_2 after 30 seconds and 60 seconds according to the GRPM at 900, 925 and 950 °C

Temperature	Extent of calcination	
	30 s	60 s
900	0.070	0.178
925	0.788	0.996
950	0.999	1.000

8. CONCLUSIONS FROM PART ONE

The kinetic of calcination reaction was studied varying the material, the temperature and the sweep gas at low CO_2 concentrations (20%vol.). The rate increases with the temperature and the reaction is completed in 15 seconds at 950 °C. Dolomite decomposes faster than limestone and the MgO content enhances its anti-sintering properties exhibiting higher conversions. Calcination under nitrogen and helium has the same rate under the same conditions.

Two models were used for describing the calcination kinetics, the Generalized Random Pore model and the Prout-Tompkins model. The GRPM fits slightly better to the experimental results especially at low conversions. A large difference was observed between the predicted values of the activation energy (GRPM: 162 kJ/mol, P-T model: 230 kJ/mol) probably due to deviations of the fitting results. The GRPM approach is more realistic due to the surface area evolution theory but needs input information from BET measurements and is more complex than P-T model.

Future plans include more experimental work on calcination kinetics, as well as the application of the two models on more data to ensure that the so far obtained information is accurate. The effect of the steam addition will also be tested and- if the technical limitations will be overcome- calcination experiments under higher CO_2 concentrations will be done.

PART TWO: KINETIC EXPERIMENTS IN A TGA (CSIC)

9. MATERIALS

The samples tested by CSIC are quite pure and show a single crystalline phase as inferred from XRD analysis (calcite in case of limestone OMYCARB 10 BE and dolomite for DOLOMITA PPS). Some relevant parameters of the materials used for the experiments described below are listed in Table 6.

10. METHODS

10.1. Calcination Isotherms

The kinetics of calcination of the samples was studied by CSIC using a Q5000IR thermogravimetric analyser (TA Instruments). This thermobalance is provided high sensitivity balance, a fast furnace heated by four infrared lamps and a small volume reactor that allows a very rapid change of atmosphere.

Calcination experiments were carried out at different temperatures under pure CO_2 and 70%vol. CO_2:30%vol. He at atmospheric pressure. The samples were initially heated at 300 °C/min from 50 °C to 800 °C and the temperature was stabilized over a period of 5 min. Then, the samples were heated up to the target temperature, which was maintained constant until the calcination process was finished. An example of these experiments is shown in Figure 15.

The reaction progress (X) has been calculated from the thermogravimetric experimental data according to equation (1):

$$X = \frac{m\%_0 - m\%}{m\%_0 - m\%_f} \qquad (1)$$

being $m\%_0$ the initial mass%, $m\%_f$ the final mass% and $m\%$ the sample mass at an instant time t.

11. RESULTS AND DISCUSSION

The experimental curves (X vs time plots) can be fitted reasonably well by using the Prout-Tompkins model, as shown in Figure 16 – Figure 28. The kinetic parameters obtained from the fits that are required to plot the PTM eq. 10 shown in Section 3.2 are shown in Table 7 and Table 8 for the experiments carried out under 70%vol. CO_2:30%vol atmosphere and under pure CO_2 atmosphere, respectively.

It should be noted that these Figures do not normalise the extent of conversion after reaction completion to 100% as the AUTH study in Part One does. Thus, the curves asymptotically approach values of X which are less than 100%.

From these results, it is inferred that the reaction rates decrease, as expected, as the calcination temperature approaches the equilibrium temperatures (870 °C for 70%vol. CO_2 and 895 °C for pure CO_2). This behaviour can be clearly observed in the X vs time plots (Figure 16 – Figure 28). Thus, it can be seen in these plots that reaction times are lower than 1 min for OMYACARB 10 BE calcined at 960 °C under pure CO_2 and about 10 minutes are needed at 935 °C for full calcination a 935 °C under the same atmosphere (Figure 20). The same behaviour is observed when calcination is carried out under 70%vol. CO_2 atmosphere.

Due to the influence of the equilibrium temperature, it could not be possible to study the calcination at the same temperature under both atmospheres. In case of dolomite, it shows faster calcination kinetics than the limestone sample, as can be inferred from the experiments performed under the same conditions (Table 7 and Table 8).

Table 6 – Purity (from XRD analysis), particle size distribution (µm) and S_{BET} (m^2/g) of samples studied by CSIC.

SAMPLE	Purity	S_{BET}	Dv(10)	Dv(50)	Dv(90)	D[3;2]	D[4;3]
OMYACARB 10 BE	Pure calcite	1.6	2.50	6.46	13.5	4.85	7.30
DOLOMITA PPS	Pure dolomite	1.3	1.06	6.70	32.1	3.12	12.4

Table 7 – PTM kinetic parameters of calcination at different temperatures under 70%vol. CO_2.

TEMPERATURE	OMYACARB 10 BE		DOLOMITA PPS	
	k (s^{-1})	t_0 (s)	k (s^{-1})	t_0 (s)
910°C	0.013	264	-	
900°C	0.0048	720	0.074	41
897°C	0.0023	1320	0.033	111
895°C	0.00083	2773	0.0092	224
893°C	-		0.0063	316
890°C	0.00067	5581	0.0030	594

Table 8 – Reaction rates (s^{-1}) of calcination at different temperatures under 100% CO_2.

TEMPERATURE	OMYACARB 10 BE		DOLOMITA PPS	
	k (s^{-1})	t_0 (s)	k (s^{-1})	t_0 (s)
960°C	0.075	32	-	
950°C	0.045	71	-	
940°C	0.030	155	-	
935°C	0.017	276	-	
930°C	0.0088	499	0.054	57
925°C	-		0.018	161
923°C	-		0.0085	254
920°C	0.00050	6469	0.005	517
915°C	-		0.00067	3508

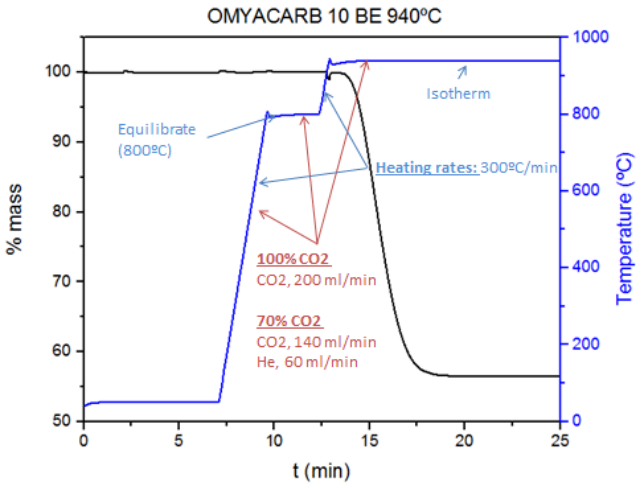

Figure 15 – OMYACARB 10 BE thermogram showing the time evolution of temperature and mass% for a typical isothermal experiment of calcination. The different stages of the experiment are shown in the figure.

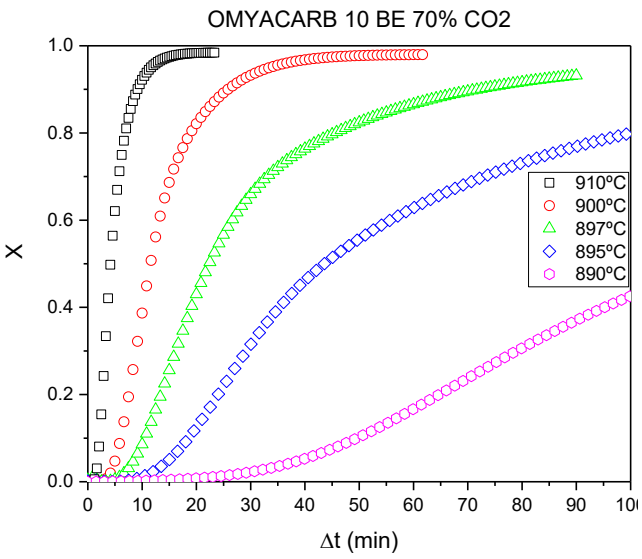

Figure 16 – X vs time plot for OMYACARB 10 BE. Calcination was carried out at different temperatures under 70%vol. CO_2

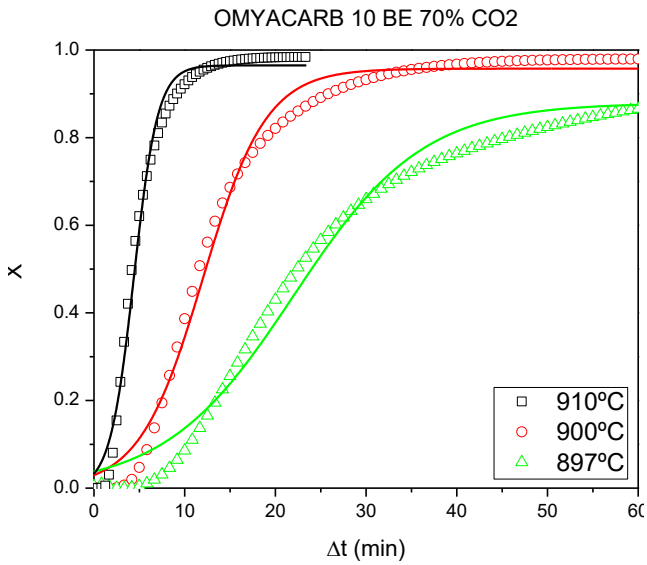

Figure 17 – X vs time plot for OMYACARB 10 BE calcined at 910 °C, 900 °C and 897 °C under 70%vol. CO_2. The symbols correspond to experimental data and the solid lines correspond to the fit to the Prout-Tompkins model.

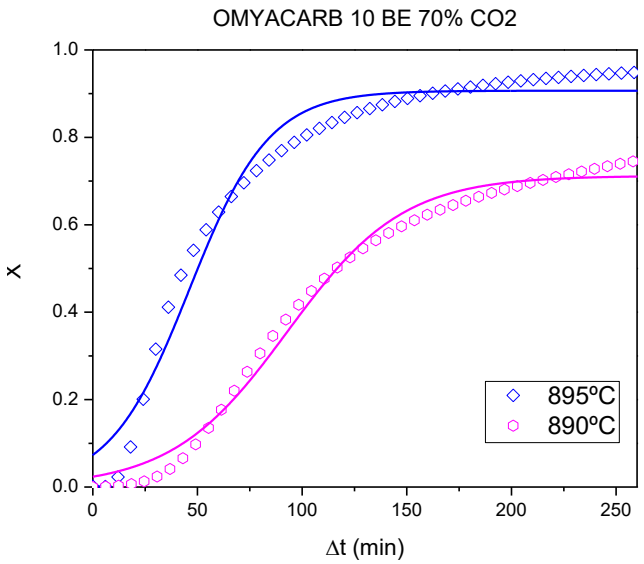

Figure 18 – X vs time plot for OMYACARB 10 BE calcined at 895 °C and 890 °C under 70%vol. CO_2. The symbols correspond to experimental data and the solid lines correspond to the fit to the Prout-Tompkins model.

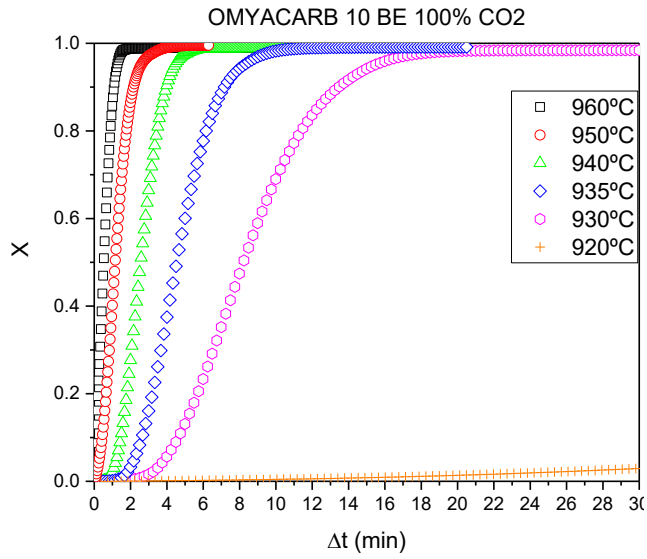

Figure 19 – X vs time plot for OMYACARB 10 BE. Calcination was carried out at different temperatures under pure CO_2.

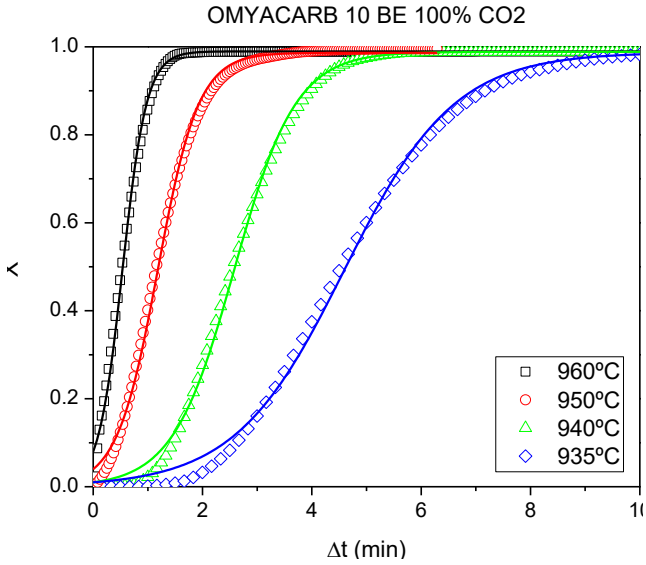

Figure 20 – X vs time plot for OMYACARB 10 BE calcined at 935 °C, 940 °C, 950 °C and 960 °C under pure CO_2. The symbols correspond to experimental data and the solid lines correspond to the fit to the Prout-Tompkins model.

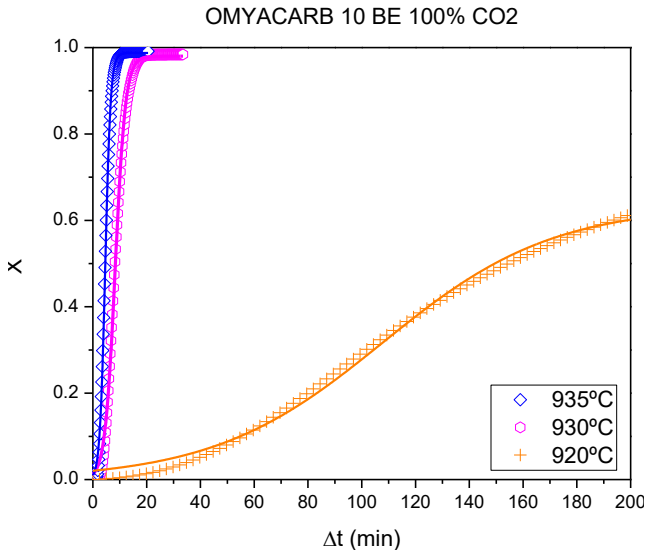

Figure 21 – X vs time plot for OMYACARB 10 BE calcined at 935 °C, 930 °C and 920 °C under pure CO_2. The symbols correspond to experimental data and the solid lines correspond to the fit to the Prout-Tompkins model.

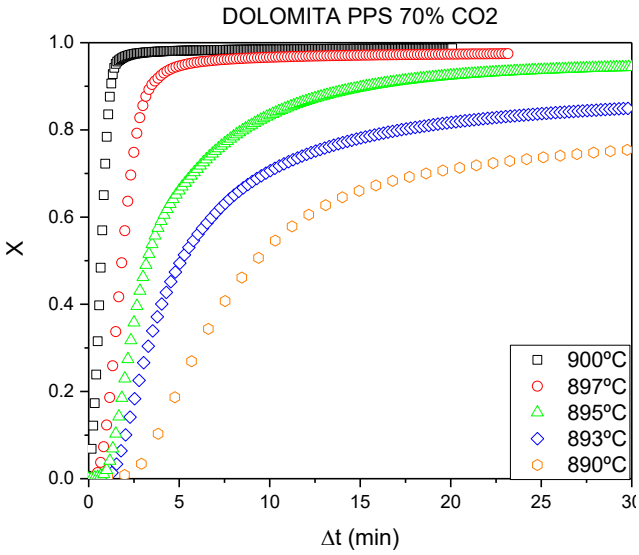

Figure 22 – X vs time plot for DOLOMITA PPS. Calcination was carried out at different temperatures under 70%vol. CO_2

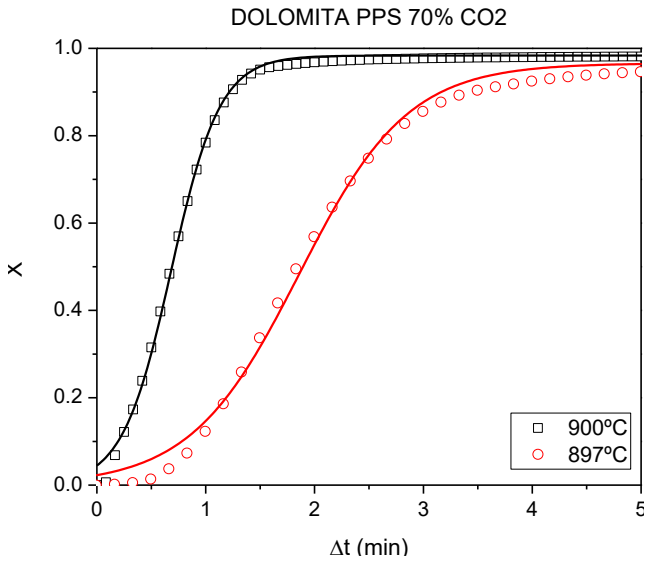

Figure 23 – X vs time plot for DOLOMITA PPS calcined at 900 °C and 897 °C under 70%vol. CO_2. The symbols correspond to experimental data and the solid lines correspond to the fit to the Prout-Tompkins model.

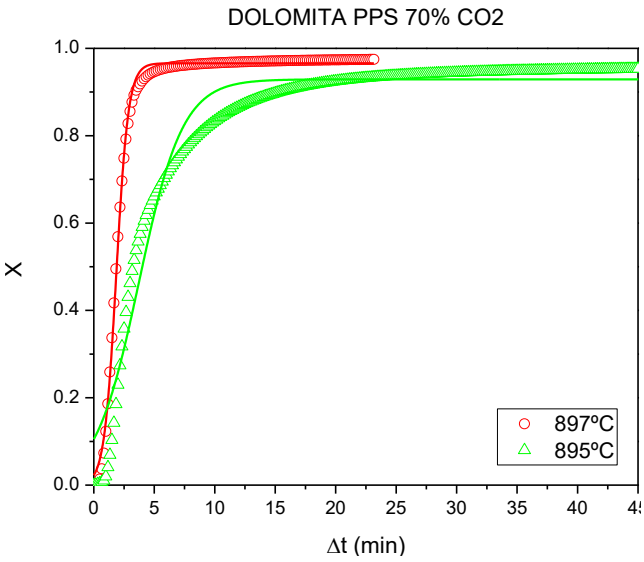

Figure 24 – Comparison of the X vs time plot for DOLOMITA PPS calcined at 897 °C and 895 °C under 70%vol. CO_2. The symbols correspond to experimental data and the solid lines correspond to the fit to the Prout-Tompkins model.

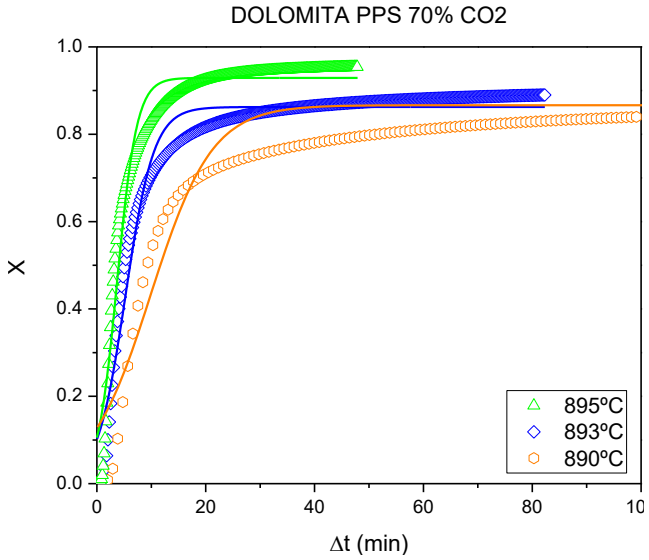

Figure 25 – Comparison of the X vs time plot for DOLOMITA PPS calcined at 890 °C, 893 °C and 895 °C under 70%vol. CO_2. The symbols correspond to experimental data and the solid lines correspond to the fit to the Prout-Tompkins model.

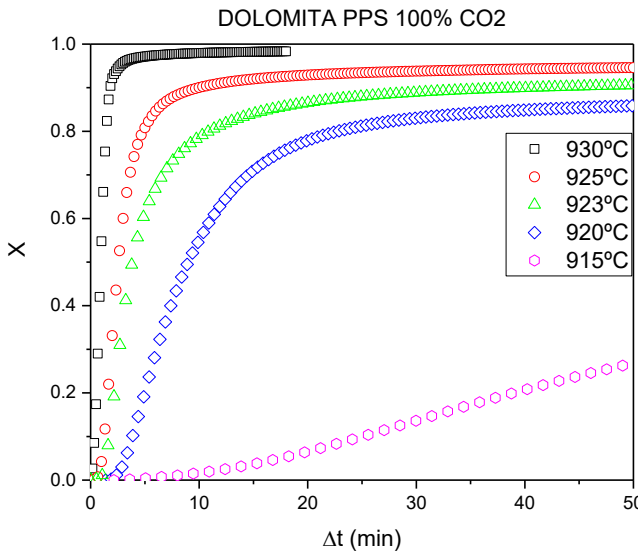

Figure 26 – X vs time plot for DOLOMITA PPS. Calcination was carried out at different temperatures under pure CO_2.

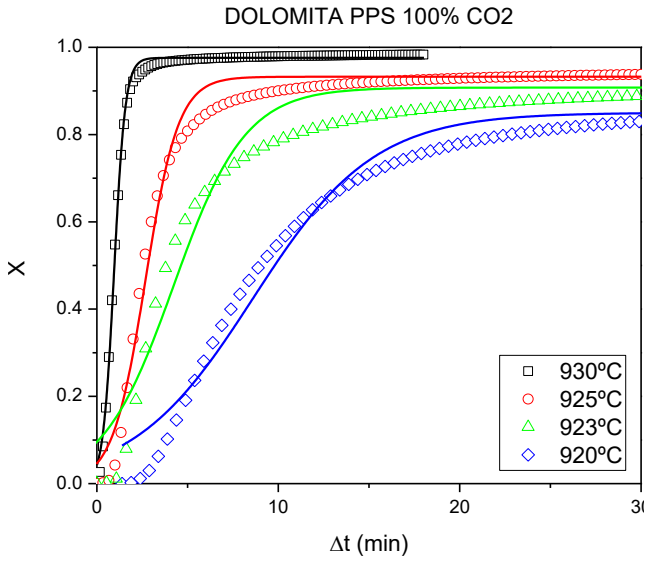

Figure 27 – X vs time plot for DOLOMITA PPS calcined at 920 °C, 923 °C, 925 °C and 930 °C under pure CO_2. The symbols correspond to experimental data and the solid lines correspond to the fit to the Prout-Tompkins model.

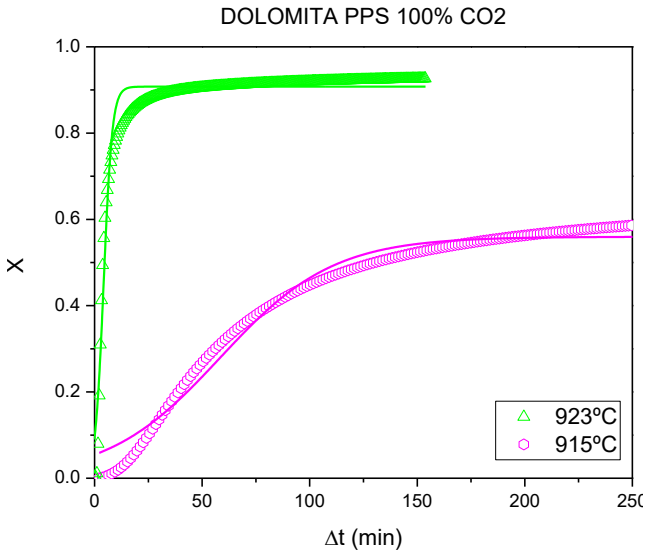

Figure 28 – Comparison of the X vs time plot for DOLOMITA PPS calcined at 923 °C and 915 °C under pure CO_2. The symbols correspond to experimental data and the solid lines correspond to the fit to the Prout-Tompkins model.

11.1. Comparison of Part One and Part Two results

It is interesting to compare these results with those of the GRPM in Part One. There are a few corrections that have to be made. Firstly, the model should take the smaller particle size in to account. Secondly, the different porosity and surface area leads to different values of pore surface area and pore diameter. However, this latter correction cannot be made due to the lack of pore volume data for Omyacarb 10BE.

Figure 19 shows calcination at 950 °C and 100% CO_2 occurring in around 4 minutes. The GRPM in The Prout-Tompkins model, although less complex, cannot predict rates of calcination in 100% CO_2 with data from only 20% CO_2 atmospheres because of the dependence on t_0, which is empirically determined.

Table 5, on the other hand, predicts virtually complete calcination (99.9%) within 30 seconds in the same conditions; this is true with the new diameter, too. At 920 °C in 100% CO_2, the limestone reaches 50% calcination in 180 minutes (Figure 21) whereas the GRPM suggests this extent of calcination would be achieved in around 22 seconds for limestone with the same diameter. This is a significant deviation which should be studied in more detail. It may be that one of the two experimental methods is constrained by something other than the kinetics, or that the GRPM is too sensitive to temperature or partial pressure of CO_2. The CaO* intermediate may also have an influence.

CONCLUSION

The Prout-Tompkins model has been used to fit experimental calcination curves registered at different temperatures under pure CO_2 and 70%vol.CO_2:30%vol. He atmosphere. The reaction rates decrease as the calcination temperatures approach the corresponding equilibrium temperatures (870 °C for 70%vol. CO_2 and 895 °C for pure CO_2).

Dolomite shows faster calcination kinetics than the limestone sample, as inferred from the experiments performed under the same calcination conditions.

PART THREE: EFFECT OF FAST CALCINATION (CERTH)

12. INTRODUCTION

This section describes a study performed at CERTH to compare the effect of fast calcination on the capacity/cycle-to-cycle stability and the kinetics of two chosen CaO-based samples. While overall the effect of 5 different parameters were/are still being studied (Figure 29), the main results presented below relate to the identification of the effect of the following 3 parameters:

- *Atmosphere*: 100% CO_2, 50% CO_2–50% He and 100% He

- *Heating Rate during calcination*: 120 °C/min, 300 °C/min, 600 °C/min and 900 °C/min

- *Maximum calcination temperature*: 900 °C and 1000 °C.

In all cases, cooling of samples – after completion of fast calcination – occurred naturally and under the same atmosphere/flow with the one employed during heating and calcination at the maximum temperature, as indicated above. Thus e.g. in the case of cooling under CO_2 containing flow, the samples were fully or mostly re-carbonated. This occurred spontaneously and without any particular control or monitoring of such re-carbonation extent.

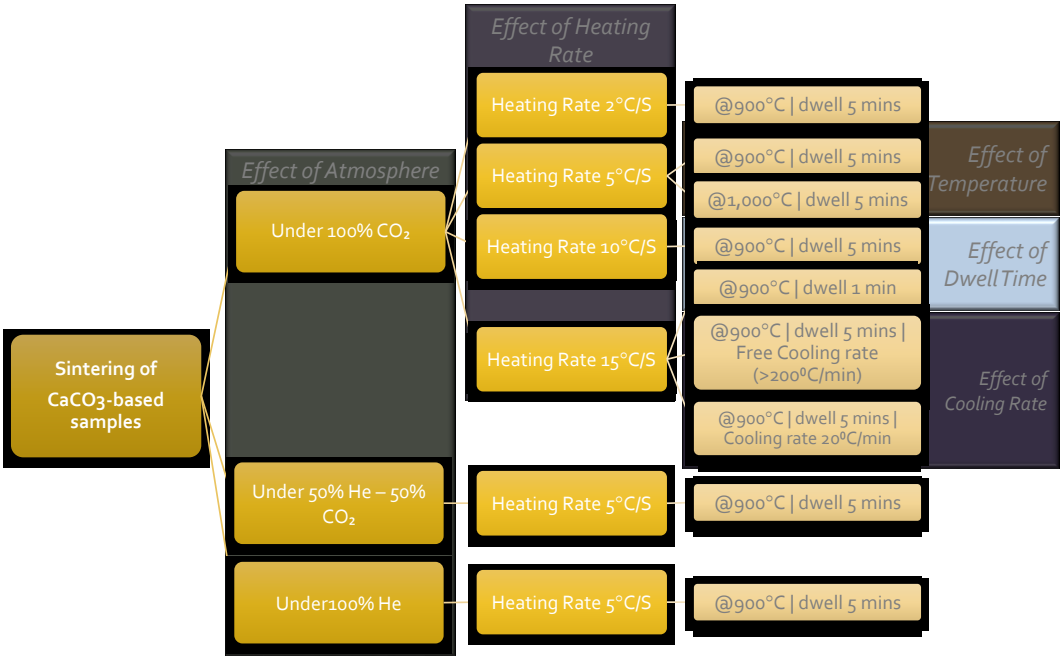

Figure 29 – Schematic of the parametric calcination (sintering) study

The main motivation of the particular studies was the identification of the impact of fast thermal treatment, typically expected to be the case under solar irradiation of CaO-based materials in the framework of the SOCRATCES concept, on the overall performance of energy storage medium.

The preliminary assessment of findings led to the exclusion of the less promising sample for further investigation. On the optimum sample, in addition to the above three parameters, the effects of ***Dwell Time*** at the maximum sintering temperature and ***Cooling Rate*** are currently under evaluation and will be reported in the future. The former relates to sample heating at the maximum temperature for 1 or 5 min, while the latter refers to the cooling of the sample according to two different protocols: in one hand free/natural cooling, with a variable rate (but constantly >200 °C/min at the temperature range where calcination/carbonation typically occur) and in the other hand a stable rate of 12 °C/min.

13. MATERIALS

Two materials are studied both acquired from OMYA: a limestone with the commercial name GRANICARB 0.1/0.8 and one dolomitic sample called MICRODOL 1-KN. The detailed physico-chemical characteristics of the particular materials have been provided in Deliverable D3.1.

14. EXPERIMENTAL SET-UP

14.1. IR Furnace

The two samples were exposed to the different fast calcination protocols with the aid of a desktop IR furnace (Figure 30) that allows for very rapid heating of the samples, i.e. nominally up to 50 °C/s or 3,000 °C/min, under controllable atmospheres.

Figure 30 – High-temperature desktop IR Furnace

14.1. Thermogravimetric Analysis

The samples, after exposure to the different calcination protocols described in Section 12 were evaluated with respect to their calcination/carbonation capacities and kinetics upon 5 consecutive cycles (Figure 31). The degree of conversion was extracted via continuous monitoring of the samples' weight with the aid of a Thermogravimetric apparatus (PYRIS TGA analyser). During the isothermal carbonation steps depicted in Figure 31 (green highlighted areas), the atmosphere was changed from 100% N_2 to 100% CO_2. The heating rate was constant at 5 °C/min and the cooling rate was set at 15 °C/min. Due to the non-monitored/spontaneous re-carbonation that occurs during the natural cooling of the fast-calcined samples in the IR-furnace, the extent of calcination and kinetic rates of fast-calcined materials in the TGA were not calculated from the first calcination step, but from the second.

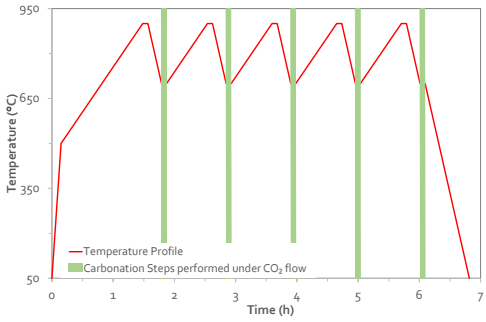

Figure 31 – Temperature profile employed as a testing protocol during consecutive calcination-carbonation cycles

15. CHARACTERIZATION

15.1. Comparison of the Non-Flashed Samples

In Figure 32 the weight change (%) and the temperature evolution during 5 consecutive cycles performed on the two samples, in their ''non-flashed'' form, are plotted as a function of time. For the case of the MICRODOL 1-KN sample, a significant difference is observed between initial weight loss and the first carbonation. In the course of the next calcination/carbonation cycles, the material shows a stable behaviour. In the case of the GRANICARB 0.1/0.8 sample, the deactivation occurs gradually and the capacity difference between the 1st and 5th carbonation is profound.

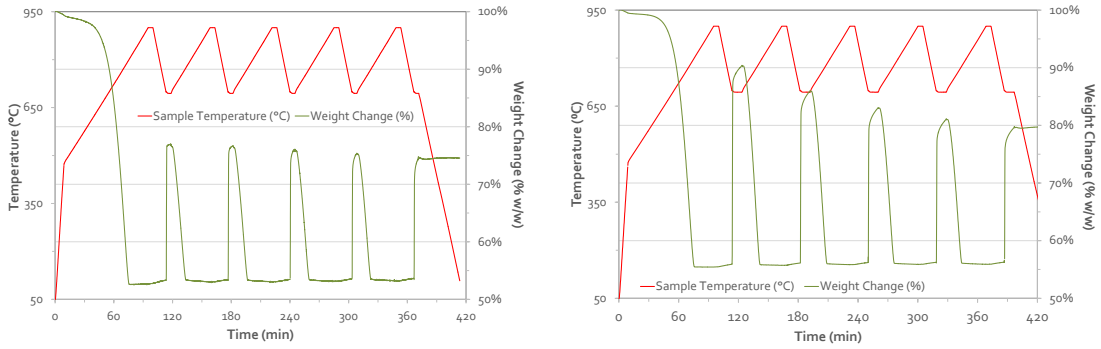

Figure 32 – Weight change evolution recorded upon 5 calcination-carbonation cycles with a) the MICRODOL 1-KN and b) the GRANICARB 0.1/0.8 samples respectively.

For the estimation of conversion degrees (Figure 33), a reasonable assumption was made that after completion of each calcination step the samples contain only the respective oxides; i.e. in the case of GRANICARB 0.1/0.8, the mass after calcination was assumed to correspond to pure CaO, whereas the respective mass of MICRODOL 1-KN, was attributed to formation of CaO and MgO, at a ratio of Ca:Mg = 1:2.3, as estimated from SEM/EDS analysis. In order to constantly have rational conversion degrees, the lowest mass recorded during the 5 cycles was correlated to the mass of pure oxides. As expected, the general trend is that the lowest mass was recorded after the 1st calcination step.

From the weight change evolution presented in Figure 32, it is obvious that the calcination reaction proceeds at almost 100%. The later observation, suggests that the "deactivation" of the samples is evident during the carbonation step only. Based on the conversion degrees presented in Figure 33, it is observed that MICRODOL 1-KN exhibits a rather low carbonation degree (47.6% in the 1st cycle) as compared to GRANICARB 0.1/0.8 (80.2%). This is due to the presence of large quantities of MgO, which does not easily carbonate under these conditions. However, MICRODOL 1-KN presents very low cycle-to-cycle deactivation (carbonation degree reduces <5 percentage units from 1st to 5th cycle) while conversion degree of GRANICARB 0.1/0.8 reduces very quickly (> 25 percentage units capacity loss from 1st to 5th cycle). Thus, it is expected that the initial conversion degree difference between the 2 samples will be eliminated within a maximum number of 8 cycles.

Based on the approximation that MICRODOL 1-KN and GRANICARB 0.1/0.8 correspond to $CaCO_3.2.33MgCO_3$ and 100% $CaCO_3$ respectively, the theoretical amount of CO_2 that can be exchanged upon calcination-carbonation cycles was calculated (Figure 34a). During both calcination and carbonation steps recorded, any mass loss/gain observed, was correlated to CO_2 released or absorbed. The amounts of CO_2 absorbed during the 1st and 5th cycles are presented as a function of time in Figure 34a, while in Figure 34b the respective carbonation rates are presented. In accordance to the conclusions drawn above, in both samples there is a deviation in the carbonation degree from the theoretical values, while during the 5th cycle the amount of

CO_2 per sample mass of GRANICARB 0.1/0.8, has become almost equal to that of MICRODOL 1-KN. With respect to the carbonation rate (Figure 34b), the reaction in MICRODOL 1-KN proceeds faster. In both cases, the carbonation rate decreases with the cycles and the difference is more profound for GRANICARB 0.1/0.8.

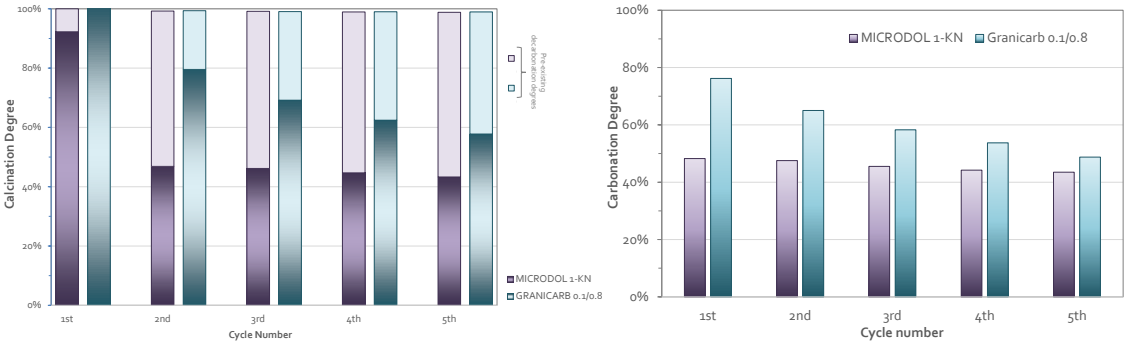

Figure 33 – Comparative bar graphs of the conversion degree recorded upon 5 calcination-carbonation cycles with the MICRODOL 1-KN and the GRANICARB 0.1/0.8 samples.

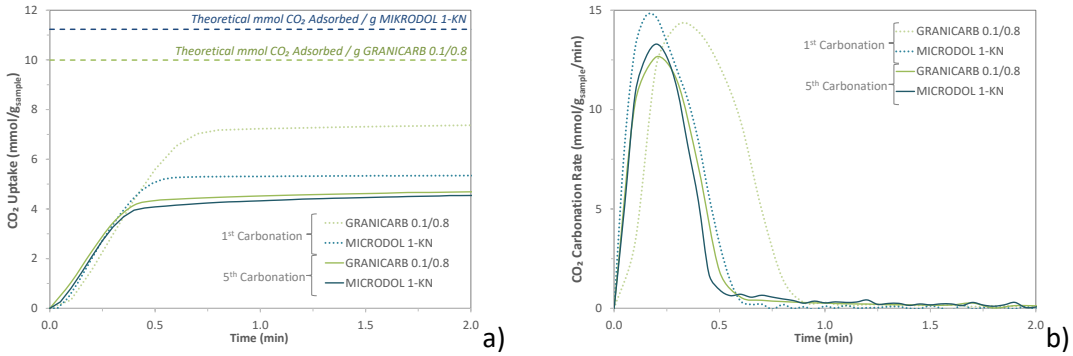

Figure 34 – Comparative evolution of a) the amount of CO_2 absorbed and b) CO_2 carbonation rate, during the 1st and 5th carbonation reactions as a function of time.

As already mentioned, the two samples presented above, were both subjected to different fast calcination protocols to study the effect of a) first calcination atmosphere, b) heating rate and c) first calcination temperature on the calcination/carbonation activity of the samples. All samples after being exposed to the selected pre-treatment protocol were evaluated via a TGA apparatus with respect to their calcination-carbonation activity.

15.2. Effect of Calcination Atmosphere

As stated above, the two samples were subjected to three different calcination atmospheres: 100% CO_2, 50% CO_2-50% He and 100% He.

In all cases the maximum calcination temperature applied was 900 °C, the heating rate 300 °C/min and dwell time of 5 min at the maximum temperature. In Figure 35, the performance of flash-calcined samples is compared to that of the untreated (non-flash calcined) ones. As it can be observed, the combination of fast calcination and different exposure atmospheres does not have any effect on the performance of GRANICARB 0.1/0.8, i.e. in all cases the cyclic deactivation pattern is essentially identical to the untreated form. This observation indicates that there is actually no point in further examining the behaviour of GRANICARB 0.1/0.8 under fast calcination conditions and thus this sample is disqualified from further such studies.

On the other hand, the fast calcination pre-treatment of MICRODOL 1-KN resulted in a measurable improvement in terms of CO_2 uptake/release cf. its "non-flash calcined" performance (Figure 35), while the associated maximum reaction rates are also enhanced substantially (Figure 36). In addition, a measurable positive effect of calcination under He-

containing atmospheres (and especially for the case of pure He) is identified, particularly during the initial carbonation/decarbonation cycle. In the course of the 5th cycle, the difference in the CO_2 uptake between the sample fast calcined under 50% CO_2-50% He and under pure He becomes negligible (<3%, Figure 35). Conversely, the clear positive effect of pure He flow on reaction rates observed during the initial fast sintering is retained up to the 5th cycle (Figure 36).

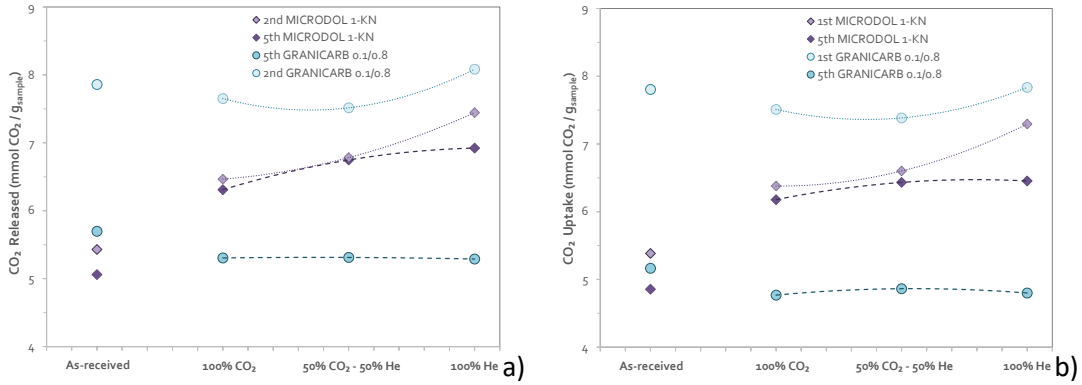

Figure 35 – Effect of sintering atmosphere on CO_2 released / up-taken during a) calcination and b) carbonation steps.

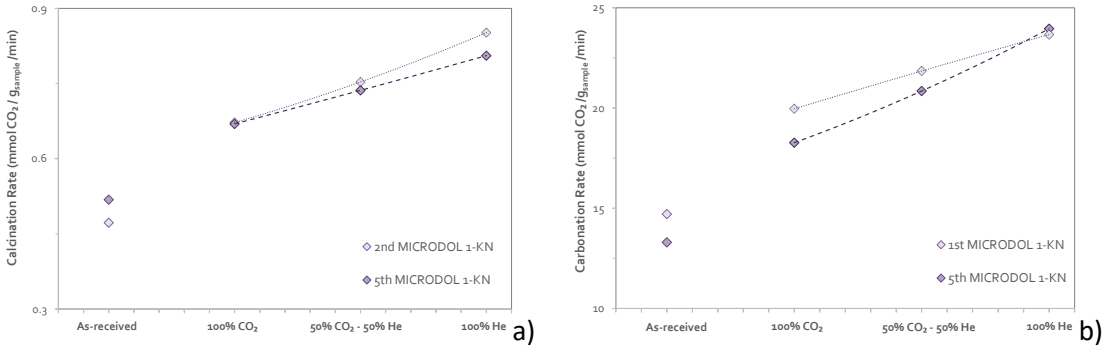

Figure 36 – Effect of sintering atmosphere on MICRODOL's 1-KN maximum reaction rates; a) CO_2 calcination rate and b) CO_2 carbonation rate.

15.3. Effect of Heating Rate

In order to study the behaviour of MICRODOL 1-KN as a function of the heating rate during fast sintering, four different values were imposed: 120 °C/min, 300 °C/min, 600 °C/min and 900 °C/min.

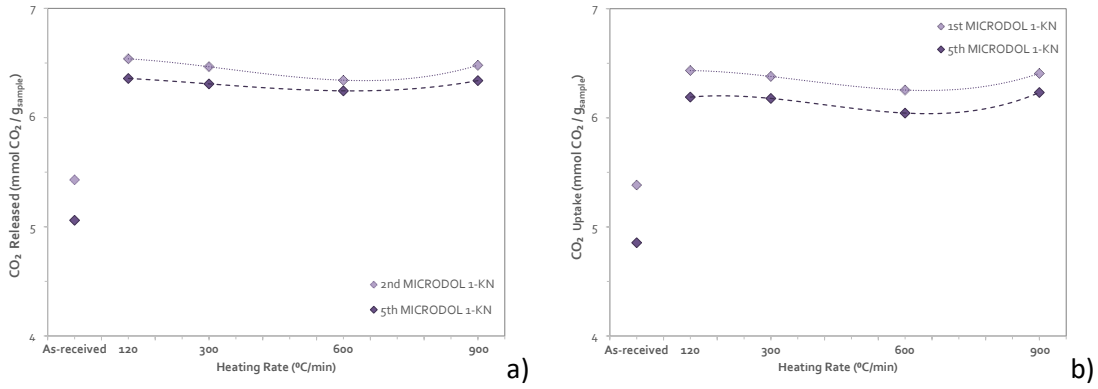

Figure 37 – Effect of heating rate during sintering on CO_2 released / up-taken during a) calcination and b) carbonation steps.

In all cases, the calcination atmosphere was 100% CO_2. Figure 37 shows the effect of the different heating rates applied on the CO_2 capacity of the samples. MICRODOL 1-KN again retains well its higher performance cf. its untreated form within the 5 cycles studied. Despite this clear positive effect, no particular trend is observed among the different fast calcination rates imposed. On an average basis and in agreement to the conclusions stated in the previous paragraph, the CO_2 release/uptake increase is approx. 22 %.

Figure 38 presents the effect of heating rate imposed on maximum carbonation/calcination reaction rates. In the case of calcination, all heating rate values led to both increase and stabilization of calcination rate, with the optimum results observed in the case of 300 °C/min. In the case of carbonation and despite the fact that the maximum rate is again observed at 300 °C/min, the degradation pattern of the non-flash calcined sample upon cycling is maintained on the flash-calcined sample as well. It can be argued that a relatively slower heating rate, i.e. 120 °C/min, may lead to a more cycle-to-cycle stable maximum carbonation rate and an increase of the absolute rate value.

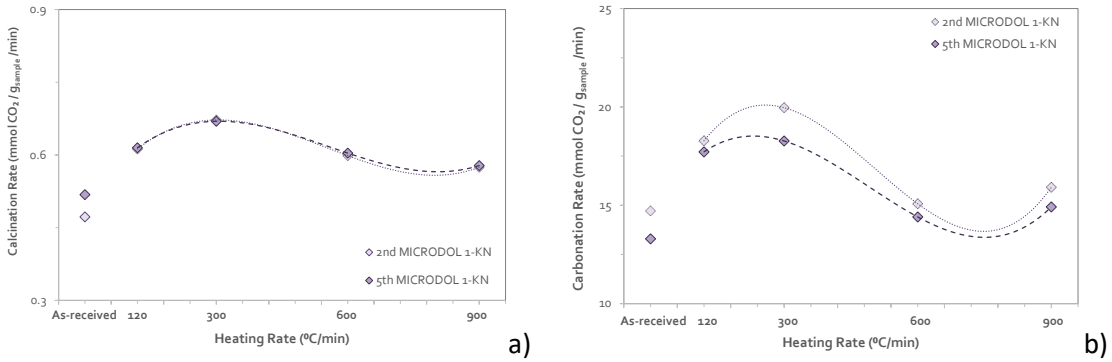

Figure 38 – Effect of heating rate during flash calcination on MICRODOL's 1-KN maximum reaction rates; a) CO_2 release rate and b) CO_2 uptake rate.

15.4. Effect of Pre-treatment Temperature

The last parameter studied is the maximum temperature during fast calcination. The two samples were exposed to two different maximum values: 900 °C and 1000 °C, in order to study the samples behaviour with respect to CO_2 capacity (CO_2 uptake/release) and maximum reaction rates.

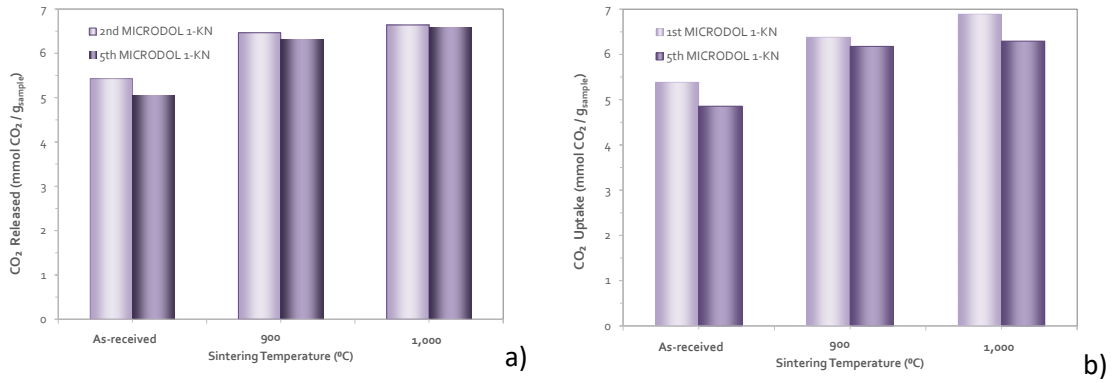

Figure 39 – Effect of pre-treatment temperature on CO_2 released / up-taken during a) calcination and b) carbonation steps.

In all cases, the heating rate during pre-treatment was 300 °C/min and the flow was 100% CO_2. Figure 39, shows the effect of the two pre-treatment temperatures on the CO_2 capacity of the samples. *MICRODOL 1-KN*, again, retains well its observed (and previously commented upon) activation via fast calcination within the 5 cycles studied. On the other hand, there is no

measurable effect of the maximum calcination temperature on either measured capacity values or maximum reaction rates.

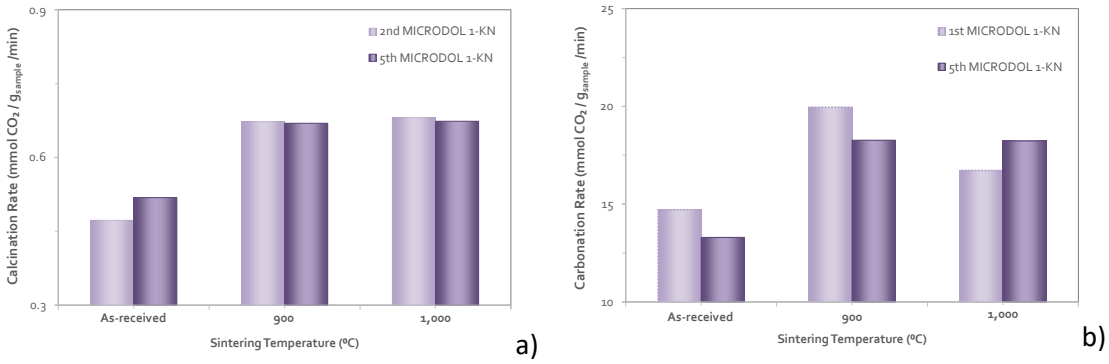

Figure 40 – Effect of pre-treatment (fast calcination) temperature on MICRODOL's 1-KN maximum reaction rates; a) calcination rate and b) carbonation rate.

16. CONCLUSIONS FROM PART THREE

Fast calcination, likely to be employed in cases of solar-aided calcination of CaO-based materials in the framework of the SOCRATCES concept, was identified as a potential effective means for further activation of one representative dolomitic sample, while it was revealed to have no measurable effect on a representative pure limestone material. Moreover, the positive effect of using He during calcination was further confirmed here, particularly with respect to carbonation/calcination maximum reaction rates calculated. Such findings indicate that dolomitic samples are very promising candidates for the particular TCES scheme studied by SOCRATCES. However, materials choice is a non-trivial task that needs to be performed in the frame of a multi-parametric study considering performance, cost, availability, toxicity & environmental-friendliness aspects.

Additional future studies, to further elaborate on the selected promising findings reported here, include quantification of the effects of cooling rate (i.e. natural vs. controlled one), as well as dwell time at maximum calcination temperature on the performance of the dolomitic sample (MICRODOL 1-KN). Moreover, CERTH will investigate the effect of multiple cycles (e.g. 5–10) under fast calcination (and natural or controlled cooling rate) on the subsequent cyclic carbonation/calcination performance in the TGA. Physicochemical characterization of untreated vs. fast calcined samples (i.e. SEM/EDS and particle size distribution) are currently underway and will be reported in the future.

17. CONCLUSIONS OF DELIVERABLE 3.2

Based on the work performed by AUTH, limestone and dolomite can calcine in the roughly 30-second timescales expected within the flash calciners at temperatures above 900 °C in 20% CO_2. The experimental results were used to calculate kinetic constants for the Prout-Tompkins Model (PTM) and Generalised Random Pore Model (GRPM). The GRPM can be used for predictive modelling, whereas using the PTM is more difficult.

The GRPM was applied to 100% CO_2 and 70% CO_2 atmospheres to effect calcination at temperatures above 900 °C. The model predicts that complete calcination will occur in a matter of seconds, similar to the experiments performed by AUTH. However, the CSIC study suggests that at those conditions such reactions may take several minutes, if not hours. The reasons for this disparity have not yet been identified but will be investigated in the next few months. This could be due to an assumption in either set of experiments or the GRPM's sensitivity to temperature and/or partial pressure of CO_2. It could relate to the intermediate species CaO*. If the current GRPM is accurate, then the current designs for the solar and electric calciners being developed in Task 3.4 should be sufficient.

Part Three shows that flash calcination is not expected to have a significant effect on the rate of calcination or the overall capacity of the limestone. However, a single initial flash calcination stage before slower cycling was found to improve the rate and capacity of the dolomite. The reasons for this are still being investigated and will be reported at a later date.

REFERENCES

[1] S. K. Bhatia and D. D. Perlmutter, “A random pore model for fluid-solid reactions: I. Isothermal, kinetic control,” *AIChE J.*, vol. 26, no. 3, pp. 379–386, May 1980.

[2] G. R. Gavalas, “A random capillary model with application to char gasification at chemically controlled rates,” *AIChE J.*, vol. 26, no. 4, pp. 577–585, Jul. 1980.

[3] M. Kendall and P. A. P. Moran, *Geometrical probability*. New York: Hafner Pub. Co., 1963.

[4] M. Sceats, “LEILAC Technical Briefing Note B4-1600-0001: The Kinetics in DS Reactors (Unpublished),” 2016.

[5] E. P. HYATT, I. B. CUTLER, and M. E. WADSWORTH, “Calcium Carbonate Decomposition in Carbon Dioxide Atmosphere,” *J. Am. Ceram. Soc.*, vol. 41, no. 2, pp. 70–74, Feb. 1958.

[6] F. García-Labiano, A. Abad, L. F. de Diego, P. Gayán, and J. Adánez, “Calcination of calcium-based sorbents at pressure in a broad range of CO2 concentrations,” *Chem. Eng. Sci.*, vol. 57, no. 13, pp. 2381–2393, Jul. 2002.

[7] Y. Wang and W. J. Thomson, “The effects of steam and carbon dioxide on calcite decomposition using dynamic X-ray diffraction,” *Chem. Eng. Sci.*, vol. 50, no. 9, pp. 1373–1382, May 1995.

[8] W. H. MacIntire and T. B. Stansel, “Steam Catalysis in Calcinations of Dolomite and Limestone Fines,” *Ind. Eng. Chem.*, vol. 45, no. 7, pp. 1548–1555, 1953.

[9] E. G. Prout and F. C. Tompkins, “The thermal decomposition of potassium permanganate,” *Trans. Faraday Soc.*, vol. 40, pp. 488–498, 1944.

[10] M. E. Brown, “The Prout-Tompkins rate equation in solid-state kinetics,” *Thermochim. Acta*, vol. 300, no. 1–2, pp. 93–106, Oct. 1997.

[11] J. M. Valverde, P. E. Sanchez-Jimenez, and L. A. Perez-Maqueda, “Limestone calcination nearby equilibrium: Kinetics, CaO crystal structure, sintering and reactivity,” *J. Phys. Chem. C*, vol. 119, no. 4, pp. 1623–1641, 2015.

[12] R. H. Borgwardt, “Calcination kinetics and surface area of dispersed limestone particles,” *AIChE J.*, vol. 31, no. 1, pp. 103–111, Jan. 1985.

[13] R. A. Bideaux, K. W. Bladh, M. C. Nichols, and J. W. Anthony, *Handbook of mineralogy Volume 4: Arsenates, Phosphates, Vanadates*. Mineral Data Pub, 2000.

[14] I. Barin and Wiley InterScience (Online service), *Thermochemical data of pure substances*. .

18. ANNEX

18.1. The Generalised Random Pore Model (GRPM)

There are two common geometry models used in the literature to describe calcination. The Shrinking Core Model (SCM) assumes that the particle is impervious, and the reaction proceeds from outer surface of the particles inwards. The Random Pore Model (RPM) assumes that the particle is porous and the reaction proceed uniformly through the particle by reaction fronts that proceed from the surface of every pore, in which there is an increase in the pore radius of the limestone as the reaction proceeds. The basic theory developed in this work is a generalisation of the RPM of Bhatia et al. [1], and Gavalas [2]. The calcination changes during the reaction because the overlap of the expanding pores evolves in a non-linear fashion, through the statistics of pore intersections [3]. The model developed below unifies the RPM with the SCM.

18.1.1. Reaction Kinetics

The first part of this paper describes the "reaction coordinates" that are relevant to the kinetics of calcination and carbonation. These properties will be derived from the Particle Size Distribution (PSD), and the Pore Volume Distribution (PVD).

The premise of the RPM is that the reaction coordinates are all the pore radii. The simplification of the model for calcination is that all the pores change radius uniformly at the same rate. With the assumption of uniform temperature and pressure, the pore radius change is also uniform within in the particle.

18.1.2. Pore Radius Change during Calcination and Carbonation

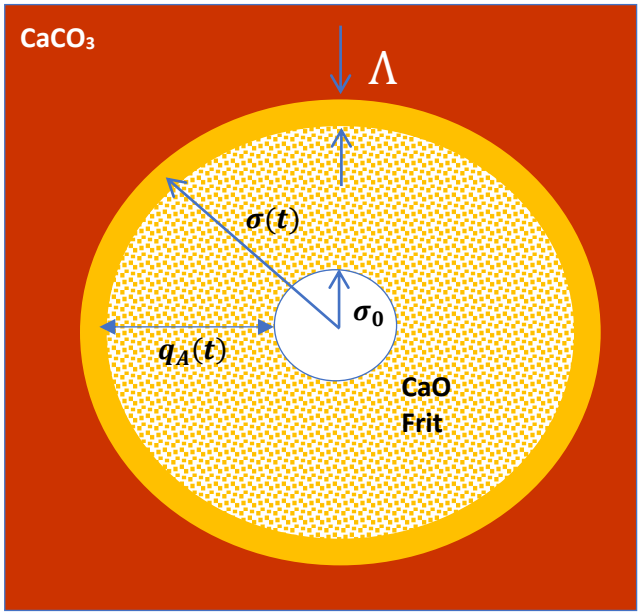

Figure 41: Pore expansion during calcination

However, a significant reaction coordinate is the depth from the initial particle surface. It is generally neglected in the RPM. The particle surface is the nominal surface of "interparticle pores". A collection of "particles" is therefore a particle in which these interparticle pores are simply another set of pores of the collection. Logically, limestone at the particle surface is no different from limestone at an internal surface (neglecting grinding effects).

The RPM asserts that all the particle pores expand at the same rate, and, self-consistently, this include the pores that are the spaces between the "particles". The reaction front for calcination for this pore moves into the particle as the reaction proceeds, and the reaction coordinate is the depth from the particle surface.

Consider first the case of calcination of an internal pore, shown in Figure 41. The initial limestone pore radius is σ_o and as calcination proceeds, the pores radius expands as $\sigma(t)$ into the $CaCO_3$ through a reaction front of width Λ. The calcination releases CO_2, and leaves behind a frit of porous CaO, which has a porosity of about 0.53 based on the molecular volumes of CaO and $CaCO_3$. The CO_2 released at the reaction front diffuses through the frit and down the original limestone pore to the surface. The extent of calcination is characterised by the pore expansion $q_A(t) = \sigma(t) - \sigma_o$, and this is the coordinate of the calcination of internal pores. The rate of pore growth is $\frac{dq_A(t)}{dt}$. The premise of the RPM is that the rate of pore growth is the same for all pores, independent of the initial pore radius. The pores in the particles are typically of the order of 0.01 to 0.1 µm in radius, and at this scale, the limestone material can be considered to be uniform.

18.1.3. Reactions from the Particle Surface

It is often observed for limestone that the calcination process occurs from the outside of the particle and proceeds inwards. This process is illustrated in Figure 42, for a particle of radius R_0.

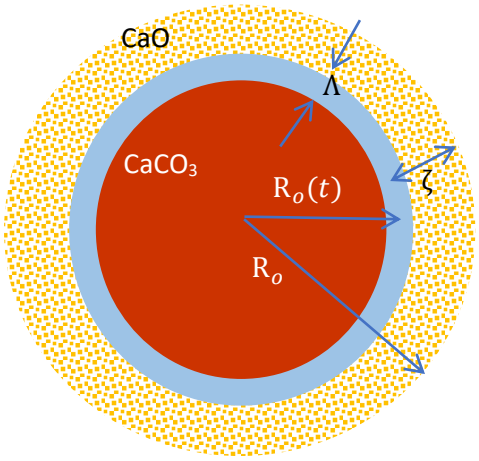

Figure 42: Reactions within a particle

The reaction front for in a particle of radius R_0 has a thickness Λ as described previously. The reaction coordinate is the depth $\zeta = R_0 - R_0(t)$ from the particle surface. ζ is the order of 0.25-50 µm for most particles, compared to the dimension of internal pores from 0.01 to 0.1 µm. It is this different length scale which leads to a difference between the calcination processes within the pores and from the surface.

In summary, the particles have two reaction coordinates for calcination, being the pore radii σ and the depth ζ from the particle's geometric surface. For a given sample, both of these coordinates have a statistical distribution, namely the Pore Volume Distribution $PVD(\sigma, \zeta)$ and the Particle Depth Distribution $PDD(\zeta)$. The dependence of the PVD on the depth formally accounts for the disorder at the surface.

18.1.4. The Depth Distribution Function and Inhomogeneous Calcination

The particles in a sample A to be calcined are characterised by a Particle Size Distribution, $PSD_A(\mathrm{d}_p)$ which measures the volume fraction of particles with effective diameters between $\mathrm{d}_p$and $\mathrm{d}_p + d\mathrm{d}_p$. (The PSD is generally derived from measurements that assume the particles are spherical.)

Rather than focussing on particle calcination for each particle size and averaging the results over a distribution of particle sizes, the GRPM analyses the surface properties of the ensemble

of particles in which the variable of interest is the depth ζ of the region of a particle from the particle surface.

In this work, the important parameter is the depth of the material from the surface of the particle. The surface area of a reaction front at depth ζ to the volume of a spherical particle of diameter d_p is

$$S(\zeta, \mathrm{d}_p) = \frac{3}{2}\frac{[\mathrm{d}_p - 2\zeta]^2}{\mathrm{d}_p^3}$$

The depth ζ is taken to be a reaction coordinate of the calcination reaction, which proceeds at a rate that is always proportional to the surface area, and at any time, all the particles are calcined to the same depth. Thus the reaction front evolution is of material A from a surface is characterised by a normalised Particle Depth Distribution function $PDD_A(\zeta)$ defined by

$$PDD_A(\zeta) = \int_{2\zeta}^{\infty} PSD_A(\mathrm{d}_p)\frac{6[\mathrm{d}_p - 2\zeta]^2}{\mathrm{d}_p^3} d\mathrm{d}_p$$

$$= \left[6\int_{2\zeta}^{\infty} PSD_A(\mathrm{d}_p)\frac{1}{\mathrm{d}_p} d\mathrm{d}_p - 24\zeta\int_{2\zeta}^{\infty} PSD_A(\mathrm{d}_p)\frac{1}{\mathrm{d}_p^2} d\mathrm{d}_p + 24\zeta^2\int_{2\zeta}^{\infty} PSD_A\frac{1}{\mathrm{d}_p^3} d\mathrm{d}_p\right]$$

It is noted that

$$PDD_A(0) = \int_0^{\infty} PSD_A(\mathrm{d}_p)\frac{6}{\mathrm{d}_p} d\mathrm{d}_p = S_g \text{ m}^2/\text{m}^3$$

where S_g is the mean geometrical surface area of the particles (in units of m^2/m^3). More generally, $PDD_A(\zeta)$ is the surface area of the reaction front at depth ζ. The specific geometrical surface area, in units of m^2/gm is given by

$$\bar{S}_g = 10^6 S_g/(1-\varepsilon_0)\rho \text{ m}^2/\text{g}$$

where ρ is the skeletal density in g cm^{-3}, namely that of calcite, and ε_0 is the particle porosity.

To illustrate the concept, the *PSD* of a ground mineral is modelled by a single Weibull distribution

$$PSD_A(\mathrm{d}_p) = \frac{k}{<d_p>}\left[\frac{d_p}{<d_p>}\right]^k exp\left\{-\left[\frac{d_p}{<d_p>}\right]^k\right\}$$

This distribution is often used to describe the PSD of ground minerals. It has a sharp cut-off and a tail of fragments. Figure 3 shows the PSD based on a $< d_p >$ = 50 µm and k = 7, and Figure 4 shows the corresponding PDD.

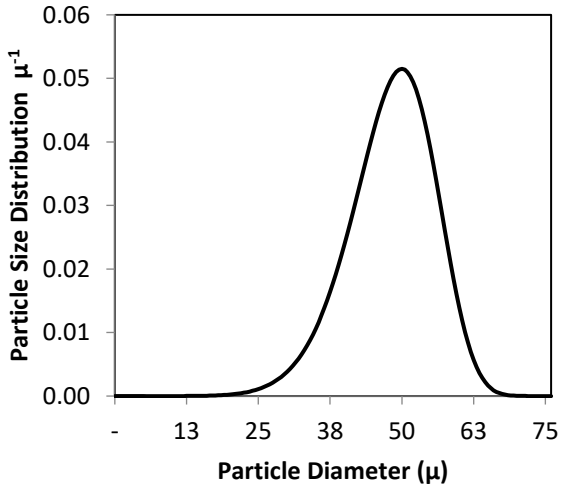

Figure 43: The Particle Size Distribution used in this study

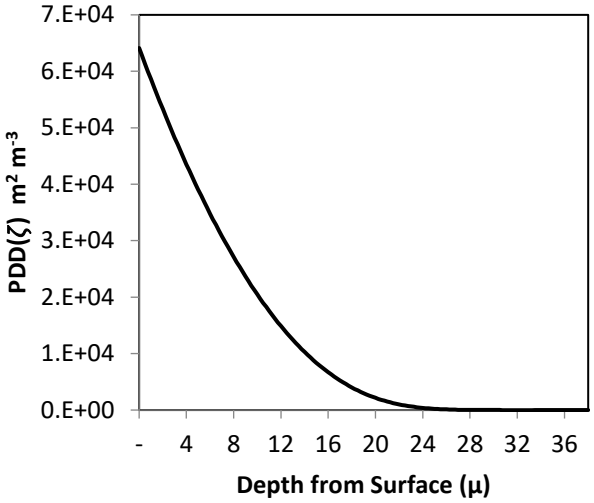

Figure 44: The Particle Depth Distribution (PDD) calculated from the PSD shown above

Particles are not spheres, and a more rigorous definition is that $PDD_A\ (\zeta)$ is the distribution of the depth of a point in the material from the nearest surface. The coordinate ζ can be regarded as a reaction coordinate. In SOCRATCES, the actual PSD of the ground sorbent used in the reactors would be used to calculate the PND and the PDD.

The degree of reaction is described by a depth dependence $\alpha(\zeta, t)$ then the average degree of calcination is given by

$$\alpha(t) = \int_o^\infty PDD_A\ (\zeta)\alpha(\zeta, t)d\zeta$$

As described above, the depth coordinate is a reaction coordinate and the reaction front at time t is defined as ζ_A. If the particle has no internal pores, the only mechanism for calcination is the growth of the reaction front from the particle surface. The calcination is given by

$\alpha(\zeta, t) = 1$ for $\zeta < \zeta_A$, $\alpha(\zeta, t) = 0$ for $\zeta < \zeta_A$ so that

$$\alpha(\zeta_A) = \int_o^{\zeta_A} PDD_A\ (\zeta)d\zeta$$

where $\alpha\left(\zeta_{A,max} = \mathrm{d}_{p.max}/2\right) = 1$.

The reaction rate at the depth ζ_A is given by

$$\frac{d\alpha(\zeta_A)}{dt} = PDD_A\ (\zeta_A)\frac{d\zeta_A}{dt}$$

As previously considered, this rate is proportional to the geometrical surface area of the reaction front at a depth ζ_A from the surface. The growth rate $\frac{d\zeta_A}{dt}$ is constant as the particle calcines under fixed conditions of temperature and pressure, and the evolution of the degree of calcination is the running integral of the PDD.

If the reaction velocity is constant, the evolution of the degree of calcination has the profile shown in Figure 6. For a single particle diameter, the evolution follows the prediction of the Shrinking Core Model (SCM) for calcination that is often used for limestone calcination. The use of the PDD is a generalisation of the SCM to account for a range of particle diameters.

In summary, the Particle Depth Distribution function $PDD_A(\zeta)$ is used to describe the calcination of particles with negligible porosity, and is a generalisation of the SCM model to deal with calcination of particles having a broad PSD.

The primary motivation for developing the PDD approach is that most experiments are carried

out using a broad distribution of particle sizes from grinding. This model allows the kinetics to be studied in a simple formulation which accounts for a broad particle size distribution.

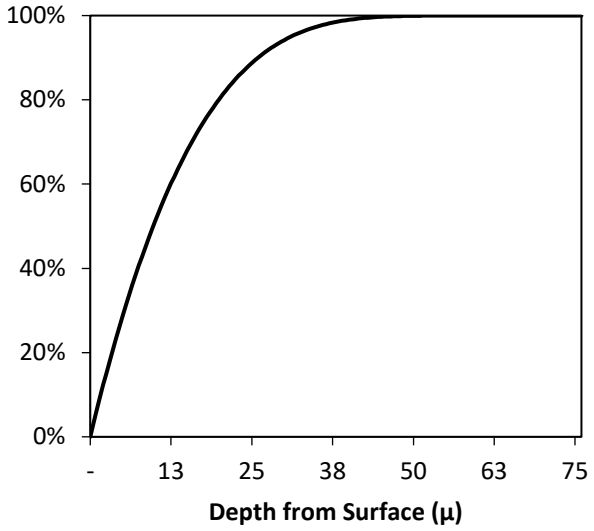

Figure 45: The running integral of the PDD mirrors the evolution of calcination from the surface

18.1.5. Internal Pores

The Random Pore Model (RPM) was originally developed by Bhatia and Perlmutter [1], and Gavalas [2] based on the statistics of random cylindrical pores for a uniform particle and a process of mass loss, such as calcination. In this work, the methodology of Gavalas is used, and is applied at any depth ζ to account for grinding effects.

Any porous particle of material A has a Pore Volume Distribution function PVD_A, $\frac{d\varepsilon_A(\sigma,\zeta)}{d\sigma}$, at a depth ζ. For convenience the minimum pore size is given as σ_{min}. When the limestone particle reacts, all the pores increase in radius by the same amount q_A, where q_A is positive for pore growth (i.e. calcination). In the GRPM, the particle boundary, counted as the "interparticle pore", also increases. The depth of the reaction front ζ_A from the particle surface competes with the internal pore expansion q_A, as an example of pore overlap statistics.

Given a material A with a distribution of cylindrical pores having a distribution of radii, the probability $\lambda_A(\sigma,\zeta,q_A)dS$ of a single intersection of a pore of radius σ with any other pore of radius $\sigma + q_A$ in a surface element dS can be evaluated when the orientation of the pores is random. The mathematics is described by Kendall and Moran [3]. The generating function $\lambda_A(\sigma,\zeta,q_A)$ and the PVD_A for a material A are related by

$$PVD_A = \frac{d\varepsilon_A(\sigma,\zeta,q_A)}{d\sigma} = 2\pi\sigma^2\lambda_A(\sigma,\zeta,q_A)exp\left[-2\pi\int_0^{\sigma_{max}}\sigma'^2\lambda_A(\sigma',\zeta,q_A)\,d\sigma'\right]$$

and

$$\varepsilon_A(\zeta,q_A) = 1 - exp\left[-2\pi\int_0^{\sigma_{max}}\sigma'^2\lambda_A(\sigma',\zeta,q_A)\,d\sigma'\right]$$

$$S_A(\zeta,q_A) = \frac{1}{1-\varepsilon_A(\zeta,q_A)}\int_0^{\sigma_{max}}\frac{2}{\sigma}\frac{d\varepsilon_A(\sigma,\zeta,q_A)}{d\sigma}d\sigma$$

$$L_A(\zeta,q_A) = \frac{1}{1-\varepsilon_A(\zeta,q_A)}\int_0^{\sigma_{max}}\frac{1}{\pi\sigma^2}\frac{d\varepsilon_A(\sigma,\zeta,q_A)}{d\sigma}d\sigma$$

The porosity, surface area and pore length are defined as m^3/m^3, m^2/m^3 and m/m^3 of skeletal material. The total porosity, surface area and pore length of the cylindrical pores are given by

$$\varepsilon_A(q_A) = \int_0^{\zeta_{max}} PDD_A\,(\zeta)\varepsilon_A(\zeta,q_A)d\zeta$$

$S_A(q_A) = \int_0^{\zeta_{max}} PDD_A\,(\zeta) S_A(\zeta, q_A) d\zeta$

$L_A(q_A) = \int_0^{\zeta_{max}} PDD_A\,(\zeta) L_A(\zeta, q_A) d\zeta$

18.1.6. Calcination

The initial $CaCO_3$ pores increase during calcination by the same amount through a mass loss. Gavalas understood that this meant that the form of $\frac{d\varepsilon_A(\sigma,\zeta,q_A)}{d\sigma}$ did not change, and the theorem of self-similarity could be applied. In this section, A refers to the residual $CaCO_3$ in a material that contains $CaCO_3$ and CaO. This means that the pore intersection probability $\lambda_A(\sigma, \zeta, q_A)$ is related to the initial pore intersection probability $\lambda_{A,0}(\sigma, \zeta, 0)$ by

$\lambda_A(\sigma, \zeta, q_A) = \lambda_{A0}(\sigma - q_A, \zeta, 0)$ for all $\zeta > \zeta_r$.

so that

$\varepsilon_A(\zeta, q_A) = 1 - exp\left[-2\pi \int_0^{\sigma_{max}} \sigma'^2 \lambda_{A0}(\sigma' - q_A, \zeta, 0)\, d\sigma'\right]$

with a change of variable, $\sigma^{"} = \sigma' - q_A$, this becomes

$\varepsilon_A(\zeta, q_A) = 1 - exp\left[-2\pi \int_0^{\sigma_{max}} (\sigma^{"} + q_A)^2 \lambda_{A0}\left(\sigma^{"}, \zeta\right) d\sigma^{"}\right]$

where

$S_A(\zeta) = \int_0^{\sigma_{max}} \frac{2}{\sigma^{"}} \frac{d\varepsilon_A(\sigma^{"},\zeta,0)}{d\sigma^{"}}\, d\sigma^{"}$

$L_A(\zeta) = \int_0^{\sigma_{max}} \frac{1}{\pi\sigma^{"2}} \frac{d\varepsilon_A(\sigma^{"},\zeta,q)}{d\sigma^{"}} d\sigma^{"}$

$S_A(\zeta)$ is the surface area of the limestone in m^2/m^3 of particles, and $L_A(\zeta)$ is the mean pore length in m/m^3 of the cylindrical pores. Expansion of the quadratic gives

$1 - \varepsilon_A(\zeta, q_A) = \left(1 - \varepsilon_A(\zeta)\right) exp[-S_A(\zeta) q_A - \pi L_A(\zeta) q_A^2]$ for $\zeta > q_A$

$\varepsilon_A(\zeta, q_A) = 1$ for $\zeta < q_A$

The evolution of the porosity change in the bulk region (neglecting the lime) is

$\frac{d\varepsilon_A(\zeta,q_A)}{q_A} = (S_A(\zeta) + 2\pi L_A(\zeta) q_A) exp[-S_A(\zeta) q_A - \pi L_A(\zeta) q_A^2]$

which gives $\left(\frac{d\varepsilon_A(\zeta,q_A)}{q_A}\right)_0 = \left(1 - \varepsilon_A(\zeta)\right) S_A(\zeta)$

The calcination at all times is defined by the parameters deduced from the initial limestone. This gives a very simple expression for the degree of calcination in the bulk material

$\alpha(\zeta, q_A) = \frac{\varepsilon_A(\zeta,q_A) - \varepsilon_A(\zeta)}{1 - \varepsilon_A(\zeta)} = 1 - exp[-S_A(\zeta) q_A - \pi L_A(\zeta) q_A^2]$ for $\zeta > \zeta_A$; $\alpha = 1$ for $\zeta < \zeta_A$

and

$\frac{d\alpha(\zeta,q_A)}{dq_A} = [S_A(\zeta) - 2\pi L_A(\zeta) q_A] exp[-S_A(\zeta) q_A - L_A(\zeta) q_A^2]$ for $\zeta > \zeta_A$

This applies for all depths where ζ_A is the depth of penetration of the reaction front into the particle. Thus the degree of calcination of the particles is given by the final $GRPM$ expression

$\alpha(\zeta_A, q_A) = \int_0^{\zeta_A} PDD_A\,(\zeta) d\zeta + \int_{\zeta_A}^{\zeta_{max}} PDD_A\,(\zeta)\, \alpha_A(\zeta, q_A)\, d\zeta.$

For homogeneous particles, the $GRPM$ for calcination gives

$\alpha(\zeta_A, q_A) = \int_0^{\zeta_A} PDD_A(\zeta) d\zeta + \{1 - exp[-S_A q_A - \pi L_A q_A^2]\} \int_{\zeta_A}^{\zeta_{max}} PDD_A(\zeta)\, d\zeta.$

The first term arises from the propagation of the reaction front from the particle surface, while the second term arises from the homogenous calcination from the internal pores of the

particle. This expression implies that there are two reaction coordinates ζ_A for the reaction from the particle surface and q_A for the reaction from the internal pores. However, these are identical. Consider the kinetics of an ensemble of particles – the space between the particles is described by a distribution of pore interparticle pores, and as calcination proceeds, the reaction front from the interparticle pores all expand at the same rate into the particle. Neglecting grinding effects, there is no inherent difference between the material near the particle surface and near a pore surface, so that $\zeta_A = q_A$. In this case, the expression becomes

$$\alpha(q_A) = \int_0^{q_A} PDD_A(\zeta)d\zeta + \{1 - exp[-S_A q_A - \pi L_A q_A^2]\} \int_{q_A}^{\zeta_{max}} PDD_A(\zeta)\, d\zeta.$$

The initial homogeneous kinetics is given by

$$\left(\frac{d\alpha(\zeta_A,q_A)}{dt}\right)_0 = \left(S_{A,g} + S_A\right)\frac{dq_A}{dt}$$

Where $S_{A,g} = PDD(0)$ is the geometric surface area, and S_A is the bulk surface area in units of m^2/m^3 of the internal pores. It is noted that measurements of the surface area using gas adsorption includes both contributions.

The important result of this paper is that the surface area for the reaction has contributions from the internal particle pores throughout the particle, and the external surface.

In summary, the final $GRPM$ expression for calcination of homogeneous particles used here is

$$\alpha(q_A) = \int_0^{q_A} PDD_A(\zeta)d\zeta + \{1 - exp[-S_A(\zeta) q_A - \pi L_A(\zeta) q_A^2]\} \int_{q_A}^{\zeta_{max}} PDD_A(\zeta)\, d\zeta.$$

which gives

$$\frac{d\alpha(q_A)}{dq_A} = \left[PDD_A(q_A) + (S_A + 2\pi L_A q_A) \int_{q_A}^{\zeta_{max}} PDD_A(\zeta)\, d\zeta\right] exp[-S_A q_A - \pi L_A(\zeta) q_A^2]$$

where $PDD_A(q_A)$ is measured from the Particle Size Distribution $PSD_A(d_p)$ and S_A and L_A are measured from the $PVD_A(\sigma)$, as measured, but formally with the particle surface contribution extracted so that the results refer to internal pores.